Cell – ECM interactions play distinct and essential roles at multiple stages during the development of the aortic arch arteries

Michael Warkala[1,2, §], Dongying Chen[3, §, ¥], Ali Jubran[3, †], AnnJosette Ramirez[1,4, †], Michael Schonning[1,4], Xia Wang[†], Huaning Zhao[4], and Sophie Astrof[1, 2, 4, *].

1. Department of Cell Biology and Molecular Medicine, New Jersey Medical School, Rutgers Biomedical and Health Sciences, Newark, NJ, USA

2. Multidisciplinary Ph.D. Program in Biomedical Sciences: Molecular Biology, Genetics, and Cancer Track, New Jersey Medical School, Rutgers Biomedical and Health Sciences, Newark, NJ, USA

3. Graduate Program in Cell & Developmental Biology, Thomas Jefferson University, Philadelphia, PA, USA

4. Multidisciplinary Ph.D. Program in Biomedical Sciences: Cell Biology, Neuroscience and Physiology Track, New Jersey Medical School, Rutgers Biomedical and Health Sciences, Newark, NJ, USA

¥ Current address: Yale Cardiovascular Research Center, Department of Internal Medicine, Yale University School of Medicine, New Haven, CT 06511, USA.

‡ Current address: Department of Anatomy, Histology & Developmental Biology, School of Basic Medical Sciences, Shenzhen University Health Science Center, Shenzhen, China

§ These individuals contributed equally to the manuscript as co-first authors

† These individuals contributed equally to the manuscript as co-second authors

Short title: Integrin $\alpha5\beta1$ and Fn1 in arch artery formation

* Corresponding author: Sophie Astrof,
sophie.astrof@rutgers.edu

185 South Orange Ave,
Medical Sciences Building, Room I-518,
Newark, NJ, 01703

Total word count: 7746
Subject Codes: Animal Models of Human Disease; Mechanisms; Vascular Biology;

Rationale: Defects in the morphogenesis of the 4th pharyngeal arch arteries (PAAs) give rise to lethal birth defects. Understanding genes and mechanisms regulating PAA formation will provide important insights into the etiology and treatments for congenital heart disease.

Objective: Cell-ECM interactions play essential roles in the morphogenesis of PAAs and their derivatives, the aortic arch artery (AAA) and its major branches; however, their specific functions are not well-understood. Previously, we demonstrated that integrin $\alpha5\beta1$ and fibronectin (Fn1) expressed in the *Isl1* lineages regulate PAA formation. The objective of these studies was to investigate cellular mechanisms by which integrin $\alpha5\beta1$ and Fn1 regulate AAA morphogenesis.

Methods and Results: Using temporal lineage tracing, whole-mount confocal imaging, and quantitative analysis of the second heart field (SHF) and endothelial cell (EC) dynamics, we show that the majority of PAA EC progenitors arise by E7.5 in the SHF and populate pharyngeal arch mesenchyme between E7.5 and E9.5. Consequently, SHF-derived ECs in the pharyngeal arches become organized into a uniform plexus of small blood vessels, which becomes remodeled into the PAAs between 31 – 35 somites. The remodeling of the vascular plexus is orchestrated by signals dependent on pharyngeal ECM microenvironment and extrinsic to the endothelium. Conditional ablation of integrin $\alpha5\beta1$ or Fn1 in the Isl1 lineages showed that signaling by the ECM regulates AAA morphogenesis at multiple steps: 1) the recruitment of the SHF-derived ECs into the pharyngeal arches, 2) the remodeling of the uniform EC plexus in the 4th arches into the PAAs; and 3) differentiation of neural crest-derived cells abutting the PAA endothelium into vascular smooth muscle cells.

Conclusions: PAA formation is a multi-step process entailing dynamic contribution of SHF-derived ECs to pharyngeal arches, the remodeling of endothelial plexus into the PAAs, and the remodeling of the PAAs into the AAA and its major branches. Cell-ECM interactions regulated by integrin $\alpha5\beta1$ and Fn1 play essential roles at each of these developmental stages.

Key Words: integrin $\alpha5\beta1$, fibronectin, second heart field, endothelial progenitor cells, pharyngeal arch arteries, aortic arch arteries

Nonstandard Abbreviations and Acronyms in the Alphabetical Order: AAA – aortic arch artery; CHD – congenital heart disease; ECs – endothelial cells; Fn1 – fibronectin; IAA-B – interrupted aortic arch type B; Itga5 – integrin $\alpha5$; PAA – pharyngeal arch arteries; RERSA – retro-esophageal right subclavian artery; SHF – second heart field; VEGFR2 – vascular endothelial growth factor receptor 2

Introduction

Aortic arch artery (AAA) and its major branches comprise an asymmetrical vascular tree that routes oxygenated blood from the heart into the systemic circulation [1]. Defects in the development of the AAA cause devastating forms of congenital heart disease (CHD) due to interruption(s) in the aortic arch, of which interrupted aortic arch type B (I-AAB) is more prevalent [2, 3]. Non-lethal defects in aortic arch morphogenesis such as vascular rings can impact the quality of life by causing constriction of the trachea and esophagus, and resulting in difficulties with eating, breathing, and also in dizziness, vertigo, or tinnitus [4].

The AAA and its major branches develop from the remodeling of three bilaterally symmetrical pairs of pharyngeal arch arteries (PAA), numbered 3, 4, and 6 [5]. It is important to note that phenotypically identical AAA defects arise due to either defects in PAA formation or defects in the remodeling of initially well-formed, symmetrical PAAs into asymmetric AAAs [6]. PAAs arise by vasculogenesis from endothelial precursors originating in the lateral plate mesoderm, also known as the second heart field (SHF) [7-13]. Experiments in zebrafish and mice have demonstrated that PAA formation is a multi-stage process that entails endothelial specification in the SHF, migration of SHF-derived endothelial progenitors into the pharyngeal region, differentiation into ECs, and the assembly of SHF-derived ECs into a plexus of small blood vessels [9, 13-16]. Thereafter, the pharyngeal endothelial plexus becomes connected with the ventral and dorsal aortae. The endothelium of the ventral aortae also forms by vasculogenesis from SHF-derived progenitors and is contiguous with the cardiac outflow tract and the PAAs [9, 11]. Following pharyngeal arch segmentation, the plexus endothelium within each arch is

102 rearranged into the PAAs [9]. The 3rd PAA is evident by E9.5, before the 4th and 6th PAAs
103 are formed. By the evening of E10.5, all three symmetrical pairs of PAAs are formed.
104 Defects in the formation of the left 4th PAA lead to I-AAB, which is lethal unless
105 corrected by surgery soon after birth [2]. Following PAA formation, neural crest-derived
106 cells closest to the PAA endothelium differentiate into vascular smooth muscle cells
107 (VSMCs), surrounding the PAA endothelium with a VSMC coat by E12.5 [17-21]. While not
108 essential for PAA formation, the differentiation of neural crest (NC)-derived cells into
109 VSMCs is essential for the stability of the PAAs, and for their eventual remodeling into
110 the asymmetrical AAA and its branches; Defects in NC differentiation in the 4th
111 pharyngeal arch lead to arch artery regression, and IAA-B [19, 20, 22]. In summary, I-AAB
112 results either due to defects in the formation of the left 4th PAA or due to its regression.

113 Morphogenesis of distinct organs and structures proceeds within niches
114 comprised of distinct complements of extracellular matrix (ECM) proteins, and
115 alterations in ECM microenvironment can severely affect embryogenesis [23-27]. We
116 discovered that the pharyngeal arch microenvironment is enriched in the ECM
117 glycoprotein fibronectin (Fn1) both at the mRNA and protein levels [28]. Fn1 is highly
118 expressed in the pharyngeal endoderm, ectoderm, endothelium, and the second heart
119 field (SHF) mesoderm between E8.5 and E10.5, the period coinciding with the time
120 when PAAs form [28, 29]. Between E10.5 and E11.5 Fn1 becomes highly upregulated in
121 the NC-derived cells abutting the 4th PAA endothelium, corresponding with the time
122 these cells differentiate into VSMCs. Our previous studies demonstrated that local
123 depletion of Fn1 in the pharyngeal microenvironment using the Isl1^{Cre} knockin mice or in
124 the NC-derived cells, using a variety of NC-expressing Cre lines, resulted in the I-AAB

125 and RERSA [29, 30]. However, mechanistically, I-AAB in these mutants had distinct
126 cellular etiology: ablation of Fn1 in using the Isl1^{Cre} knockin mice led to defective
127 formation of the 4th PAAs [29], while the ablation of Fn1 in the NC resulted in the
128 regression of originally well-formed 4th PAAs [31].

129 Integrins are a major class of transmembrane receptors that engage in signal
130 transduction upon binding ECM proteins. Integrins are heterodimers of α and β chains.
131 There are 18 α and 8 β subunits encoded by mammalian genomes, giving rise to 24
132 different $\alpha\beta$ combinations [32]. Integrin α5 complexes with integrin β1, forming the integrin
133 $\alpha5\beta1$ heterodimer [33]. Integrin $\alpha5\beta1$ binds the ECM glycoprotein fibronectin (Fn1), and
134 regulates Fn1 assembly *in vivo* [34]. Phenotypes resulting from either global or cell-type-
135 specific ablations of integrin α5 (MGI gene symbol: Itga5) or Fn1 in mice are similar [26,
136 28, 29, 31, 34-41], indicating that integrin $\alpha5\beta1$ is a major Fn1 signal transducer *in vivo*.
137 Previously, we demonstrated that the expression of integrin $\alpha5\beta1$ and Fn1 in the Isl1
138 lineages was required for the formation of the 4th PAA and the deletion of either integrin
139 α5 or Fn1 in using the Isl1^{Cre} knockin strain resulted in IAA-B [29]. To understand the
140 mechanisms by which integrin $\alpha5\beta1$ and Fn1 regulate AAA development, we analyzed
141 SHF and endothelial cell dynamics in integrin $\alpha5^{f/-}$; Isl1^{Cre} and Fn1$^{f/-}$; Isl1^{Cre} mutants
142 during PAA formation and remodeling, spanning embryonic days (E) E9.5 - E11.5 of
143 development. Our studies point to the essential roles of cell-ECM interactions mediated
144 by integrin $\alpha5\beta1$ and Fn1 at multiple stages of PAA formation and remodeling.

145

146 **Methods**

147 **Animals** All experimental procedures were approved by the Institutional Animal Care
148 and Use Committee of Rutgers University and conducted in accordance with the
149 Federal guidelines for the humane care of animals.

150 **Tamoxifen injections** *Isl1*^{MerCreMer} knockin mice [42] and Mef2C-AHF-DreERT2
151 transgenic mice [43] were used for temporal labeling of vascular progenitors in the SHF.
152 Tamoxifen was dissolved either in corn oil or in sesame oil at the concentration of 10
153 mg/ml. Labeling was done by injecting 300 μl of stock solution into pregnant females at
154 multiple time points specified in the legend to Fig. 1. E0.5 was designated to be at noon
155 on the day when the vaginal plug was found.

156 **Whole Mount Immunofluorescence staining** Labeling with BrdU, TUNEL, and
157 staining with antibodies were performed as described [29], and analyzed using IMARIS
158 (Bitplane, USA) [9, 44]. Detailed procedures for staining, analysis and cell quantification is
159 described in [44].
160

161 **Statistics** Statistical analyses were performed using Prism 8 software version 8.4.3.
162 Specific statistical tests are indicated in figure legends.
163

164 **Results**

165 **SHF contributes harbors PAA progenitors between E7.5 and E9.5.** Previous work
166 from our lab demonstrated that in the mouse, the majority of PAA endothelium is
167 derived from the SHF, derived from either Mef2C-AHF-Cre- or Isl1^{Cre}- expressing
168 mesodermal lineages [9]. To define the temporal window during which the SHF

169 mesoderm harbors endothelial progenitors of the PAAs, we used *Isl1*^{MerCreMer} knockin
170 mice [42] and Mef2C-AHF-DreERT2 transgenic mice [43] combined with pulses of tamoxifen
171 to lineage-label the SHF mesoderm at different developmental times (Fig. 1). Tamoxifen
172 was injected at discrete time points between E6.75 – E9.75, and embryos were
173 dissected at E10.5 and stained to detect lineage labeling in the pharyngeal arches.
174 Entire pharyngeal regions were imaged using confocal microscopy to quantify the
175 contribution of lineage-labeled cells to the PAA endothelium (Fig. 1, panels A-A2). The
176 expression of VEGFR2 and ERG were used to mark EC cell membrane and nuclei [45].
177 The labeling of the cardiac outflow tract and the right ventricle using *Isl1*$^{MerCreMer/+}$ mice
178 was evident at all stages tested, indicating that our labeling technique was consistent
179 with previous studies (data not shown) [42]. Myocardial cells derived from the SHF are
180 labeled when tamoxifen is injected as early as E6.5 in *Isl1*^{MerCreMer} knockin mice [42],
181 however no PAA ECs were labeled when tamoxifen was injected at E6.75 in this strain
182 (Fig. 1B) or at E7.25 in Mef2C-AHF-DreERT2 transgenic strain (Fig. 1C), suggesting
183 that PAA EC progenitors arise later in the SHF relative to cardiomyocyte progenitors.
184 The peak labeling of the PAA endothelium occurred when tamoxifen was injected at
185 E7.25 in *Isl1*^{MerCreMer} strain (Fig. 1B) and at E8.0 in Mef2C-AHF-DreERT2 strain (Fig.
186 1C). While tamoxifen injection into *Isl1*^{MerCreMer} resulted in sparse labeling of PAA ECs,
187 the injection of tamoxifen into Mef2C-AHF-DreERT2 transgenic mice led to the labeling
188 of a much larger proportion of ECs in the PAAs (compare Fig. 1B with Fig. 1C). These
189 differences likely reflect that the MerCreMer transgene is present in a single copy as it is
190 knocked into the *Isl1* locus [42], while Mef2C-AHF-DreERT2 is a transgenic strain
191 containing multiple copies of the Mef2C-AHF-DreERT2 transgene [43]. In addition, the

192 expression of *Is1* is downregulated commensurate with endothelial differentiation [46].
193 Thus, potentially low levels of *MerCreMer* expression in EC precursors could have
194 resulted in low labeling of endothelial progenitors in *Isl1*^{MerCreMer} mice relative to Mef2C-
195 AHF-DreERT2 strain. The difference in the timing of peak EC labeling in the PAAs
196 between *Isl1*^{MerCreMer} and Mef2C-AHF-DreERT2 strains is likely due to the earlier onset
197 of *Isl1* expression compared with the expression of the MEF2C-AHF-DreERT2
198 transgene; in fact, Isl1 regulates the expression of Mef2C and the activation of the
199 Mef2C-AHF enhancer [47, 48]. Correspondingly, our experiments demonstrate that the
200 peak endothelial labeling of PAAs in *Isl1*^{MerCreMer} strain precedes that of Mef2C-Dre-
201 ERT2 strain by 18 hours (compare Fig. 1B with Fig. 1C). Interestingly, the accrual of
202 SHF-derived ECs into the 4th arch continues past E8.5 as more SHF-derived cells are
203 labeled in the 4th PAAs than in the 3rd and 6th when tamoxifen is injected at E8.5 and
204 E9.5 (Fig. 1B1, 1C1). Thus, our labeling experiments show that the SHF mesoderm
205 harbors PAA endothelial progenitors between approximately E7.5 and E9.5 of
206 embryonic development.
207
208 To analyze the contribution of the SHF to the PAA endothelium quantitatively and to
209 compare two mouse strains commonly used to label the SHF, we imaged the entire
210 pharyngeal arch region corresponding to arches 3, 4, and 6, and quantified the
211 proportion of SHF-lineage labeled ECs in the PAAs from E10.5 embryos derived from
212 Isl1^{Cre} knockin and Mef2C-AHF-Cre transgenic lines (Fig. 2). The majority of SHF-
213 derived cells in the pharyngeal arches 3 – 6 are in the endothelium at 37somites, as
214 seen in sections through the pharyngeal arch region (Fig. 2A – B). Each PAA is

215 comprised of a similar number of ECs (Fig. 2C). However, there were differences in
216 PAA labeling among embryos isolated from Isl1^{Cre} and Mef2C-AHF-Cre mice (Fig. 2D,
217 E). In the constitutive *Isl1^{Cre}* knockin strain, the SHF contribution to the 3rd and 4th PAA
218 endothelium was 79$\pm$6% and 77$\pm$10%, respectively, and 57$\pm$12% to the 6th PAA (Fig.
219 2D). While the SHF contribution to the 3rd PAA was 45$\pm$8% in MEF2C-AHF-Cre
220 transgenic line, which is significantly different from *Isl1^{Cre}* knockin strain ($p<10^{-5}$, one-
221 way ANOVA with Tukey's correction for multiple testing). The SHF contribution to the
222 PAA endothelium of the 4th and 6th PAAs were similar between the two strains ($p>0.2$,
223 one-way ANOVA with Tukey's correction for multiple testing). The difference in the
224 contribution of the SHF to the 3rd PAA between the two strains likely reflects the earlier
225 onset of Cre expression in the *Isl1^{Cre}* knockin strain relative to MEF2C-AHF-Cre
226 transgenic line [47]. These data suggest that about half of the 3rd PAA progenitors arise
227 and leave the SHF prior to the activation of Mef2C-AHF-Cre. These data also indicate
228 that the deletion of one Isl1 allele, as in the *Isl1^{Cre}* knockin strain, does not impair the
229 contribution of the SHF to the PAA endothelium. In summary, our data show that the 4th
230 PAAs differ from the 3rd and the 6th PAAs in the timing during which SHF cells are
231 added, and differ from the 6th PAA in the proportion of SHF-derived cells.
232
233 **Cell-ECM interactions mediated by integrin α5β1 specifically regulate the accrual**
234 **of SHF-derived cells into pharyngeal region.** Studies described above together with
235 our previous work [9] have established a framework for the analyses of EC dynamics and
236 their genetic regulation during the morphogenesis of AAA and its major branches. Our
237 previous studies demonstrated that the deletion of either integrin α5 or Fn1 in the Isl1

238 lineages resulted in the defective formation of the 4th PAAs at E10.5, and consequently,
239 IAA-B and retro-esophageal right subclavian artery (RERSA), in these mutants [29]. I-AAB
240 and RERSA are anomalies resulting from defective morphogenesis of the left and right
241 4th PAAs, respectively [1, 3]. To determine the mechanisms by which integrin $\alpha5\beta1$ and
242 Fn1 regulate the formation of the 4th PAAs, we analyzed PAA development at distinct
243 stages of embryonic development using whole-mount immunofluorescence followed by
244 quantitative analyses of SHF-derived populations and their dynamics.

245

246 PAAs form through the coalescence of pharyngeal arch EC plexus [9, 10]. All pharyngeal
247 arch ECs are located within a plexus of small blood vessels at E9.5. At E10.5 (33 – 34
248 somite stage), 50% of the 4th arch endothelium is found within the PAA (the vessel
249 surfaced in green in (Fig. 3B, C) and 50% is in the plexus (pink in Fig. 3B, C) [9]. About
250 50% of integrin $\alpha5^{f/-}$; Isl1^{Cre} mutants have defective 4th PAAs, and consequently, 50% of
251 these mutants develop IAA-B and RERSA [29] . We found that 4th PAA is absent in 50%
252 of mutants at 32 – 34 somites (Fig. 3D – F). Instead, the endothelium in the 4th arches is
253 in the form of a plexus of small blood vessels (marked in pink in Fig. 3E, F). A small 4th
254 PAA eventually formed in these mutants by 36 – 39 somites (Fig. 3J, marked in green in
255 Fig. 3K, L; compare with the 4th PAA surfaced in green in control Fig. 3G-I). Similarly,
256 the formation of the 4th PAA was delayed in Fn1$^{f/-}$; Isl1$^{Cre/+}$ mutants (Sup. Fig. 1). This
257 defect was specific to the 4th PAA, as the 3rd and 6th PAAs formed normally in the
258 mutants (vessels surfaced in white and red in Fig. 3). The incidence of IAA-B and
259 RERSA is 50% in integrin $\alpha5^{f/-}$; Isl1^{Cre} and Fn1$^{f/-}$; Isl1$^{Cre/+}$ mutants, which is the same as

260 the incidence of defective 4th PAAs at E10.5 [29]. Therefore, we further investigated the
261 mechanisms by which integrin $\alpha5\beta1$ and Fn1 regulate the formation of the 4th PAAs.

262 We hypothesized that the defective formation of the 4th PAAs in our mutants could be
263 due to insufficient EC numbers, defective EC proliferation, or survival. To test these
264 hypotheses, we evaluated total EC numbers in the 4th pharyngeal arches of controls
265 and mutants. To quantify EC number, we stained E10.5 embryos with the antibodies to
266 ERG, a transcription factor enriched in the endothelia and either VEGFR2 or Pecam 1,
267 expressed on EC surface, as described [44]. These experiments showed that integrin $\alpha5^{f/-}$
268 ; $Isl1^{Cre}$ and $Fn1^{f/-}$; $Isl1^{Cre/+}$ mutants had decreased total number of ECs in the 4th arches
269 at 32 – 33 somites relative to controls (Fig. 3M and Sup. Fig. 1A-C). Despite this
270 decrease in EC numbers, the size of the 4th arches, the tissues within which PAAs form,
271 was not affected (Fig. 3N). EC proliferation in the 4th arch was also not affected in the
272 mutants (Fig. 3O), and neither was cell survival (Sup. Fig. 2). Thus, EC deficiency in the
273 4th pharyngeal arches of the mutants was not due to defective cell proliferation or
274 survival. The majority of $VEGFR2^+$ cells in the pharyngeal arches of E9.5 embryos were
275 labeled with GFP (Sup. Fig. 3A – A2, B – B2), indicating that SHF cells in the
276 pharyngeal region of the mutants were not impaired in the acquisition of EC fate.
277 VEGFR2 is expressed the 4th pharyngeal arch endothelium at E9.5, which is a day
278 earlier than Pecam 1 [10]. To determine whether the maturation of pharyngeal arch ECs
279 was affected in the mutants at E10.5, we co-stained embryos with antibodies to
280 VEGFR2 and Pecam 1. Despite defective 4th PAA formation, all $VEGFR2^+$ cells in
281 pharyngeal arches of the mutants also expressed Pecam1 at E10.5 (Sup. Fig. 3C, D,

282 C1, D1), ruling out maturation as a cause for decreased EC numbers in the 4th
283 pharyngeal arch.

284 Since the maturation, proliferation, and survival of ECs were not affected in our mutants,
285 we tested the hypothesis that defective recruitment of progenitor cells into the
286 pharyngeal arches was the cause for decreased EC numbers in the 4th arch. As we
287 established before, the majority of PAA endothelium arises from the SHF (Fig. 2D, E
288 and [9], and the accrual of SHF-derived cells into the pharyngeal arches is mostly
289 complete by E9.5 (Fig. 1B-C). To quantify the number of SHF-derived cells in the
290 pharyngeal mesenchyme, we used ROSA$^{nT\text{-}nG}$ reporter mice, in which nuclear
291 localization sequences were fused with tdTomato and EGFP, leading to the expression
292 nuclear-localized EGFP upon Cre-induced recombination. We found that

293 the deletion of integrin α5 in the Isl1 lineages impaired the accrual of SHF cells into the
294 pharyngeal region (Fig. 4A-B), while the accrual of SHF-derived cells into the heart was
295 not affected (Fig. 4C).

296 Splanchnic mesoderm within the dorsal pericardial wall harbors both cardiac and
297 vascular progenitors. To test whether the deficiency in the pharyngeal SHF-derived
298 mesoderm was due to the decrease in SHF cells numbers in the splanchnic mesoderm,
299 we used IMARIS to surface cells within this region and quantified the number of GFP^{+}
300 cells (see Sup. Fig. 4 for details on surfacing). These experiments showed that the
301 number of GFP^{+} cells in the splanchnic mesoderm within the dorsal pericardial wall was
302 similar between controls and mutants (Fig. 4D). Next, we computed the proportion of
303 GFP^{+} cells in the pharyngeal mesenchyme or in the heart relative to the number of

304 GFP$^+$ cells in the splanchnic mesoderm. While the latter ratio was not affected in the
305 mutants (Fig. 4E), the former was significantly decreased in the mutants (Fig. 4F),
306 suggesting that there is a defect either in the specification of pharyngeal progenitors in
307 the SHF or in their exit from the SHF. Taken together, these experiments indicate that
308 ECM microenvironment sensed through the signaling by integrin $\alpha5\beta1$ is important for
309 the accrual of the SHF-derived mesoderm to the pharyngeal arches (Model in Fig. 8,
310 PAA formation panel A1).

311

312 **Integrin $\alpha5\beta1$ and fibronectin regulate the remodeling of pharyngeal plexus into**
313 **the 4th PAAs independently of EC numbers.** Interestingly, the number of SHF-derived
314 cells and ECs in the mutants recovered by the 34-35 somite stage, and was similar to
315 that of controls (Fig. 5A). Total number of GFP$^+$ cells also recovered (Fig. 5B). The
316 percentage of GFP$^+$ ECs in the pharyngeal arches of controls and mutants were
317 comparable (Fig. 5C), indicating that the recovery was not due to the recruitment of ECs
318 from an alternative mesodermal source. The recovery of pharyngeal EC numbers was
319 likely mediated through the proliferation of SHF-derived ECs. The basis for this
320 conclusion is the following. The proliferation index of pharyngeal arch ECs was
321 unaltered in the mutants (Fig. 3O), and the proliferation index of ECs in the pharyngeal
322 plexus is 2-fold higher than that of PAA ECs, both in controls and in mutants (Fig. 3O,
323 plexus). Since the proportion of ECs in the pharyngeal plexus is higher in the mutants
324 than in controls (Sup. Fig 1D), the higher proliferation index of plexus ECsin the mutants
325 is likely responsible for EC recovery. Our quantitative analyses indicate that PAA
326 formation phenotypes in integrin $\alpha5^{f/-}$; Isl1$^{Cre/+}$ and Fn1$^{f/-}$; Isl1$^{Cre/+}$ mutants are

327 indistinguishable from one another (Sup. Fig. 1), suggesting that integrin $\alpha5\beta1$ is a
328 major receptor transducing Fn1 signals within the pharyngeal microenvironment.

329 Despite the recovery of EC numbers (Fig. 5A), PAAs remained thin in integrin $\alpha5^{f/-}$;
330 $Isl1^{Cre}$ and $Fn1^{f/-}$; $Isl1^{Cre/+}$ mutants (Fig. 3G – L), and there was 2 – 3-fold decrease in
331 the proportion of pharyngeal arch ECs in the 4th PAAs at all stages analyzed at E10.5
332 (Fig. 6A). The size of the 4th PAA increases between 32 – 39 somites, as more ECs are
333 added to the PAA from the plexus (Sup. Fig. 5), and is reflected in the percent of
334 pharyngeal arch ECs in the PAA [9]. In controls, plexus ECs in the 4th arch begin
335 coalescing into the PAA when embryos reach between 31 and 32 somites [9] (Sup. Fig.
336 5). These rearrangements result in an initially thin 4th PAAs, in which approximately
337 50% of the pharyngeal arch ECs are in the plexus and 50% in the PAA at 32 – 34
338 somite stage [9]. As the development proceeds, by 36-39 somite stage, > 60% of the 4th
339 pharyngeal arch endothelium becomes incorporated into the 4th PAA [9]. Thus, the
340 percentage of the pharyngeal arch endothelium in the 4th PAA can be taken as a
341 measure of PAA formation. The higher the proportion, the larger the PAA [9].

342 To understand the mechanisms by which integrin $\alpha5\beta1$ and Fn1 regulate the
343 remodeling of the uniform endothelial plexus into the PAA in the 4th arch, we examined
344 EC dynamics in control and mutant embryos at three time points, corresponding with 32
345 – 33 somites, 34 – 35 somites, and 36 – 39 somites. These stages span about 6 hours
346 on the 10th day of mouse embryonic development. The formation of the 4th PAAs lagged
347 in mutants relative to controls at all time points tested during E10.5 (Fig. 6A and Sup
348 Fig. 1D, E), and 7 of the 16 embryos analyzed contained only a plexus of ECs and
349 lacked the 4th PAAs at the 32 – 34 somite stage (Sup. Fig. 1E), a stage at which over

350 50% of the 4th arch endothelium in controls is located within the 4th PAAs [9] (Fig. 6A and
351 Sup Fig. 1E).

352 Since mutant embryos had fewer ECs in the 4th pharyngeal arches compared with
353 controls prior to the 36th somite stage, we performed correlation analyses to test the
354 hypothesis that the formation of the 4th PAAs depended on the total EC number or EC
355 density in the 4th pharyngeal arches. As described above, the percentage of pharyngeal
356 arch ECs in the PAA relative to the plexus can be taken as a measure of PAA formation
357 (Sup. Fig. 5) [9]. Thus, for these analyses, we quantified EC numbers in control embryos
358 isolated between 32 to 39 somite stages and plotted them against the percent of ECs in
359 the 4th PAAs (Fig. 6B). Despite the sharp, over a 3-fold increase in the number of ECs in
360 the 4th arches between these stages [9], the formation of the 4th PAAs was independent
361 of the total EC number in the 4th pharyngeal arch tissue (Fig. 6B) or EC density (Fig.
362 6C) in controls throughout the 10th day of embryonic development. Similarly, correlation
363 analysis of PAA formation in the mutants with defective (thin) and normal 4th PAAs,
364 showed that similar to controls, the rearrangement of plexus ECs into the PAA did not
365 depend on the number of total number of ECs in the 4th pharyngeal arches of mutants
366 (Fig. 6D).

367 Next, we compared PAA formation in controls and mutants that had a similar number of
368 ECs in the 4th pharyngeal arches (Fig. 6E). These analyses showed that in groups of
369 mutant and control embryos with a similar number of ECs, the percent of ECs in the
370 PAAs was lower in the mutants (boxes in Fig. 6E). These data indicate that the
371 reorganization of the plexus ECs into the PAA in the 4th pharyngeal arch does not
372 depend on the EC number at E10.5, and is regulated by factors extrinsic to the

373 pharyngeal arch endothelium. In summary, our studies indicate that during the 10th day
374 of embryonic development, cell – ECM interactions mediated by integrin $\alpha5\beta1$ and Fn1
375 are essential for the remodeling of the initially uniform vascular plexus into the PAA in
376 the 4th pharyngeal arches (Model in Fig. 8, PAA formation panel A2).

377

378 **The expression of integrin $\alpha5$ in the Isl1 lineage is required for the differentiation**
379 **of neural crest cells into vascular smooth muscle cells.**

380 In the Tbx1$^{+/-}$ mouse model of 22q11 deletion syndrome, PAA formation recovers in 50
381 – 68% of the mutant mice [49, 50]. To determine whether the rearrangement of the
382 endothelial plexus in the 4th arch was blocked or delayed, we examined E11.5 embryos.
383 The incidence of IAA-B and RERSA in integrin $\alpha5^{f/-}$; Isl1^{Cre} mutants is 50%, which is the
384 same as the incidence of defective 4th PAA formation. Therefore, we expected to find
385 absent or thin 4th PAAs in the mutants at E11.5. Contrary to our expectations, the
386 formation of the 4th PAAs recovered in the mutants by E11.5, and PAA perimeters in the
387 mutants were comparable with controls (Fig. 7A, n=8). Consistent with the recovery of
388 SHF-derived ECs numbers by 33 – 35s, PAA ECs were GFP^{+} cells in the mutants as in
389 controls (compare Fig. 7C1 with 7D1, arrowheads). Regression of left 4th PAAs results
390 in IAA-B and regression of the right 4th results in RERSA [51, 52]. Since 50% of *integrin*
391 *$\alpha5^{flox/-}$; Isl1^{Cre}* mutants develop 4th arch artery defects, such as IAA-B and RERSA [29],
392 these data indicated that the 4th PAAs eventually regress in the mutants. Arch artery
393 regression is commonly caused by the defective differentiation of neural crest cells
394 surrounding the PAA endothelium into vascular smooth muscle cells, VSMCs [52-57]. In

395 pharyngeal arches, VSMCs exclusively arise from NC-derived cells [49, 58, 59]. To
396 determine whether the differentiation of NC-derived cells into VSMCs was affected in
397 our mutants, we analyzed VSMC differentiation in the pharyngeal arches. For these
398 experiments, we calculated the fraction of vessel perimeter covered by alpha smooth
399 muscle actin (αSMA)-expressing cells, using previously-developed methodology [31]. We
400 found that the differentiation of NC-derived cells into VSMCs was severely diminished
401 around the PAAs in the mutants (quantified in Fig. 7B; compare sections in Fig. 7C, D,
402 magnified in Fig. 7C2, D2; zoom-out panels are in Sup. Fig. 6). The decrease in αSMA
403 expression was not due to NC cell death (Sup. Fig. 2).

404 Even though, the *Isl1* lineage marks a subset NC-derived cells [60], Isl1 protein is not
405 expressed in NC-lineage cells in the pharyngeal arches, and Isl1 lineage does not label
406 cells adjacent to the PAA endothelium (Fig. 7C1, D1) [29]. Moreover, comparison of NC
407 lineage (Fig. 7E – E4) and Isl1 lineage maps at E11.5 demonstrates that αSMA
408 expression coincides with the NC lineage (Fig. 7E2), but not with Isl1 lineage-labeled
409 cells (arrows in Fig. 7C1 and C2 point to αSMA-expressing cells; arrowheads point to
410 GFP^+ PAA endothelium). These studies indicate that the expression of integrin α5 in the
411 Isl1 lineage(s) regulates the differentiation of NC cells into VSMCs in a non-cell
412 autonomous manner. These results are consistent with our previous experiments
413 demonstrating that the expression of integrin α5 in the *Mesp1* lineage marking the
414 anterior mesoderm regulates the differentiation of NC cells into VSMCs around the 4th
415 PAA [59]. Since the deletion of integrin α5 in the *Mesp1* lineage does not result in
416 defective or delayed PAA formation [59], these data taken together, indicate that the
417 defect in VSMC differentiation in *integrin* $\alpha 5^{flox/-}$*; Isl1*^{Cre} mutants is not merely due to the

418 delayed accrual of arch artery endothelium, or delayed remodeling of the vascular
419 plexus into the PAA. In summary, our studies also indicate that in addition to regulating
420 4th PAA formation, integrin α5 expressed in the *Isl1* lineages plays an independent role
421 in arch artery morphogenesis, namely in the differentiation of NC-derived cells into
422 VSMCs (Fig. 8A).

423 The differentiation of NC into VSMCs is orchestrated in part by a relay of Notch
424 signaling transduced from the PAA endothelium to the surrounding layers of NC-derived
425 cells [56]. The activation of Notch signaling in the NC is required for the differentiation of
426 NCs into VSMCs [52, 56]. We demonstrated that this pathway was regulated by the
427 expression of integrin α5 and fibronectin specifically by NC-derived cells at E11.5 [31]. To
428 test the possibility that the expression of integrin α5 in the *Isl1* lineages regulates the
429 lateral propagation of Notch from the PAA endothelium to the adjacent NC-derived cells,
430 we stained control and mutant sections with an antibody to Notch Intracellular Domain
431 (NICD), an activated form of Notch. However, Notch signaling was activated
432 comparably in controls and mutants, despite the severe deficiency in the differentiation
433 of NC cells into VSMCs in the mutants (compare Fig. 7C2 – C4 with Fig. 7D2 – D4,
434 arrows). These experiments indicate that the expression of integrin α5 in the pharyngeal
435 arch mesoderm regulates the differentiation of NC cells into VSMCs independently of
436 Notch. Furthermore, these experiments indicate that while the activation of Notch is
437 necessary for the differentiation of NC-derived cells into VSMCs, it is not sufficient.
438 Taken together, with our previous work [31, 59], studies in this manuscript demonstrate that
439 cell-ECM interactions regulated by integrin α5β1 and Fn1 play multiple, pleiotropic, and
440 stage-specific functions during the morphogenesis of the 4th PAAs (Fig. 8).

441 **Combinatorial expression of integrin α5 and fibronectin from multiple lineages in**
442 **the pharynx regulates the formation of the 4th PAAs.**

443 The *Isl1* lineages encompass the mesoderm in the SHF and pharyngeal arches,
444 pharyngeal endoderm, surface ectoderm, and some NC-derived cell populations,
445 although not the NC in the pharyngeal arches [29, 42, 59, 60]. Our previous studies indicated
446 that the combined expression of integrin α5β1 or Fn1 in the surface ectoderm and the
447 NC was not required for the formation of the 4th PAAs [29, 31]. However, even though PAA
448 formation occurred normally in these mice, the 4th PAAs regressed later due to defects
449 in the differentiation of NC-derived cells into VSMCs, resulting in RERSA and IAA-B [31]
450 (Fig. 8). The expression of either integrin α5β1 or Fn1 in the SHF lineage marked by the
451 expression of the Mef2C-AHF-Cre transgene is also not required for PAA formation
452 (Sup. Tables 1 and 2), indicating that the expression of integrin α5β1 or Fn1 in the SHF
453 alone is not required for cardiovascular development. Consistent with these findings, the
454 expression of integrin α5β1 in the *Mesp1* lineage or in the endothelium was not required
455 for PAA formation [59, 61] (Fig. 8). Instead, the expression of integrin α5β1 in the Mesp1
456 lineage was required for PAA stability, and the deletion of integrin α5 in *Mesp1* lineage
457 which includes the PAA endothelium resulted in IAA-B and RERSA (Fig. 8) [59, 61].

458 The difference in the phenotypes resulting from the deletion of integrin α5 using Mef2C-
459 AHF-Cre and Mesp1^{Cre} are likely the result of differences in the timing of Cre expression
460 (e.g. the later onset of Mef2C-AHF-Cre may have allowed the perdurance of integrin
461 α5β1 protein through the stages where it's required for mesoderm-NC interactions).
462 Alternatively, the expression of integrin α5β1 in Mesp1 lineage-derived mesodermal

463 cells prior to E8.5 is important for the regulation of NC cell fate in the pharyngeal arches
464 [59].

465 Lastly, we tested whether the expression of integrin α5 in the endoderm regulated PAA
466 formation. For these experiments, we used the constitutive Sox17$^{2A\text{-}iCre}$ knockin mouse
467 line, in which Cre is expressed in the endoderm and pharyngeal arch ECs (Sup. Fig. 7A
468 – A4) [62]. However, PAAs formed normally in *α5$^{flox/-}$;* Sox17$^{2A\text{-}iCre}$ mutants (Sup. Fig. 7B,
469 B1, C, C1). Together, these data indicate that combinatorial expression of integrin α5
470 and Fn1 in the Isl1 lineages is necessary for the proper formation of the 4th PAAs (Fig.
471 8).

472

473 **Discussion**

474 Proper development of the 4th PAAs is central to the ability of a newborn to survive and
475 thrive (Karunamuni et al., 2014; Moon, 2008). The formation of the 4th pair of the PAAs
476 is regulated by a number of genes including *Tbx1, Pax9, Gbx2, Fgf8, Crkl, PlexinD1,*
477 *and Nrp1*, e.g., [63-67]. However, cellular mechanisms by which these genes mediate PAA
478 formation are not well-understood. Unraveling the dynamics of EC progenitors and their
479 descendants during PAAs formation is vital to understanding the genetic and cellular
480 mechanisms regulating PAA formation and how they are altered in congenital heart
481 disease.

482 In this manuscript, we have demonstrated that the SHF is the primary source of the
483 PAA endothelium and that the majority of endothelial progenitors giving rise to the PAAs

484 are already present in the SHF by E7.5. PAA progenitors exit the SHF and contribute to
485 the PAAs over a span of about 2 days, from E7.5 to E9.5.

486

487 Lineage labeling using constitutive Cre lines Isl1^{Cre} and Mef2C-AHF-Cre led to similar
488 labeling of the PAA endothelium, with the exception of the 3rd PAA, which is labeled
489 50% more efficiently when Isl1^{Cre} line of mice is used. This difference likely reflects the
490 timing of Cre expression in Isl1^{Cre} and Mef2C-AHF-Cre strains, with Mef2C-AHF-Cre
491 lagging by about a day [42, 48, 68]. This suggests that about half of the endothelial
492 progenitors of the 3rd PAA have exited the SHF by the time Mef2C-AHF-Cre is
493 expressed. Our fate mapping studies show that there are differences in the timing and
494 the extent of SHF contribution to the PAAs. In particular, if one were to use Mef2C-AHF-
495 Cre to generate mutations, the 4th PAAs could be more affected than the 3rd and the 6th
496 because in the MEf2C-AHF-Cre strain, the contribution of the SHF lineage-labeled ECs
497 to the 4th PAA endothelium is the highest.

498 By using whole-mount imaging and quantitative analyses of EC populations in the
499 pharyngeal arches, we previously demonstrated that the morphogenesis of the 4th PAAs
500 occurs gradually throughout the 10th day of the embryonic development and entails a
501 rapid accumulation of ECs: endothelial population in the 4th pharyngeal arch increases
502 more than three-fold in about eight hours of development, from 30 – 39 somites [9]. This
503 steep increase is unlikely to occur solely due to EC proliferation, and our labeling
504 experiments show that SHF-derived cells are still being added to the 4th PAA after E9.5.

505 Our studies show that integrin $\alpha5\beta1$ and Fn1 are important for initial recruitment of SHF-
506 derived ECs into the 4th pharyngeal arches, and that in the absence of integrin $\alpha5$ or
507 Fn1 in the Isl1 lineages results in EC deficiency up to 32 – 34 somite stage. Despite the
508 initial EC deficiency in the 4th arch, EC numbers recover in integrin $\alpha5^{f/-}$; Isl1$^{Cre/+}$ and
509 Fn1$^{f/-}$; Isl1$^{Cre/+}$ mutants by the 34 – 35 somite stage. We demonstrate that the recovery
510 of EC cell numbers in the pharyngeal arches is not due to compensation from an
511 alternative endothelial source. Instead, we show that the proliferation index of plexus
512 endothelium is 2-fold higher than that of ECs in the PAA (Fig. 3O). This difference in the
513 proliferation index is maintained in the mutants (Fig. 3O). We hypothesize that since the
514 majority of ECs is in the plexus in the mutants at 32 – 33 somites, their proliferative
515 advantage over ECs in the PAA allows the EC number in the mutant arches to recover
516 by the end of E10.5.

517 However, in spite of the recovery of EC populations in the 4th arches, the 4th PAAs were
518 either thin or absent in 50% of all the 4th arches by 36 – 39 somite stages [29]. Our
519 regression analysis showed that the rearrangement of the 4th pharyngeal arch ECs into
520 the PAA was not dependent on the number or density of ECs in the 4th arch. These data
521 suggest that the remodeling of the uniform endothelial plexus into the PAA in the 4th
522 arch is mediated by factors extrinsic to the endothelium. The disruption of the
523 remodeling in our mutants indicates an essential role for cell – ECM interactions in this
524 process.

525

526 The *Isl1* lineage encompasses multiple cell types within the pharynx including
527 pharyngeal epithelia, mesoderm, and a population of NC cells in the cardiac outflow
528 tract [60, 68]. Pharyngeal endoderm and the ectoderm are important signaling centers
529 regulating intercellular communications among the germ layers composing the arches,
530 the endoderm, mesoderm, surface ectoderm and the neural crest, mediating the
531 morphogenesis of cardiopharyngeal organs and structures [27, 69, 70]. Modulation of the
532 extracellular microenvironment within the pharynx is essential for the development of
533 the heart, the AAA and its branches [29, 31, 59, 63, 64, 71-81]. The expression of *Fn1*, an
534 essential ECM glycoprotein, is highly enriched in the pharyngeal epithelia and Fn1
535 protein is enriched in the pharyngeal arches 3 – 6 [28, 29]. Our studies show that the
536 expression of Fn1 in the Isl1 lineages is important for the formation of the 4th PAAs,
537 while Fn1 expression in the NC regulates PAA stability [29, 31] (Fig. 8).

538

539 In this manuscript, we investigated the tissues wherein signaling by Fn1 is important for
540 PAA formation. Integrin $\alpha5\beta1$ is a major Fn1 receptor during embryogenesis [28-30, 34, 38,
541 39, 41], and the deletion of integrin $\alpha5$ or Fn1 in the Isl1 lineages results in identical
542 phenotypes [29]. To determine the cell type(s) in which signaling by Fn1 regulates PAA
543 formation, we ablated integrin $\alpha5$ in each of the tissues comprising Isl1 lineage
544 individually or in combination. The deletion of integrin $\alpha5$ in the SHF (Mef2C-AHF-Cre
545 strain), the entire anterior mesoderm (Mesp1^{Cre}), the NC (Wnt1-Cre2, P3Pro-Cre), the
546 NC and surface ectoderm (TFAP2$\alpha^{IresCre}$), or the endoderm and endothelia (Sox17$^{2A-iCre}$)
547 resulted in normal PAA formation (this study and [29, 31, 59]). Therefore, we conclude

548 that combinatorial signaling by integrin $\alpha5\beta1$ from pharyngeal endoderm, mesoderm,
549 and the surface ectoderm is essential to mediate the formation of the 4th PAAs. While
550 signaling in the mesoderm and the neural crest is important for PAA stability (Fig. 8).

551

552 The PAAs form within the neural crest-derived pharyngeal mesenchyme and the PAA
553 endothelium induces the differentiation of the adjacent NC-derived cells into VSMCs [56].
554 Despite the initial delay in the formation of the 4th PAAs, the size of PAAs in integrin $\alpha5^{f/-}$
555 ; Isl1$^{Cre/+}$ mutants has recovered by E11.5. At this time, we observed a profound
556 deficiency in the expression of αSMA by NC-derived cells around the PAAs in the
557 mutants. Deficiency in VSMC differentiation causes vessel regression [31, 52, 57, 82, 83],
558 consistent with our findings that integrin $\alpha5^{f/-}$; Isl1$^{Cre/+}$ and Fn1$^{f/-}$; Isl1$^{Cre/+}$ mutants
559 develop IAA-B and RERSA, defects that are caused by the aberrant morphogenesis of
560 the left and right 4th PAAs, respectively [29]. Our previous studies using integrin $\alpha5^{f/-}$;
561 Mesp1$^{Cre/+}$ mice demonstrated that the expression of integrin $\alpha5$ in the mesoderm
562 regulates NC differentiation into VSMCs without affecting PAA formation, and integrin
563 $\alpha5^{f/-}$; Mesp1$^{Cre/+}$ mice develop IAA-B and RERSA [59] (Fig. 8). Thus, the roles of integrin
564 $\alpha5\beta1$ and Fn1 in the formation of the 4th PAAs are separate from their roles in the
565 differentiation of NC-derived cells into VSCMs [31].

566

567 Mechanisms that lead to IAA-B are complex but generally arise due to either of the
568 following two broad categories of defects: a) defects in the formation of the left 4th PAA
569 or b) defects in the stability of an otherwise well-formed 4th PAA. NC ablation studies in

570 chick and genetic manipulation of the neural crest demonstrate that NC is not required
571 for PAA formation [51, 52]. Even in the extreme case of neural crest ablation, PAAs form [51].
572 However, defective differentiation of NC-derived cells into VSMCs leads to PAA
573 regression resulting in various malformations in the aortic arch and its branches,
574 including IAA-B and RERSA [31, 52, 82]. Our studies show that the expression of integrin
575 $\alpha5\beta1$ in the pharyngeal mesoderm and the NC are required for NC-to-VSMC
576 differentiation, and the expression of integrin $\alpha5\beta1$ in either of these lineages alone is
577 not sufficient for this process [31, 59].
578

579 Defects in the formation of the 4th PAAs often occur in conjunction with 22q11 deletion
580 syndromes [84]. Cumulatively, four prospective studies found that between 40 and 90% of
581 interrupted aortic arch type B (IAA-B) cases diagnosed in fetuses, neonates, and
582 children can be attributed to deletions in the 22q11 region [85]. Studies using *Tbx1*$^{+/-}$ mice
583 that model 22q11 deletion syndrome indicated that defective formation of the left 4th
584 PAA underlies IAA-B in these patients [65, 86, 87]. Intriguingly, several independent
585 publications demonstrated that *Tbx1* regulates the expression of integrins and
586 extracellular matrix (ECM) components, and showed that defects in cell-ECM
587 interactions downstream of *Tbx1* precede pathological sequelae and cardiovascular
588 defects in *Tbx1* mutants [71-73]. Interestingly, about 50% of Tbx1$^{+/-}$ mice recover from the
589 initial defect in PAA formation, and are viable and fertile [50]; However, this recovery can
590 be impeded by the reduction in the expression of Fn1 [49]. Thus, alterations in cell-ECM
591 interactions and pharyngeal ECM microenvironment may underlie lethal AAA defects in
592 22q11 deletion syndrome downstream of *Tbx1*.

593 The significance of our work lies in the identification of cellular dynamics regulating PAA
594 formation and the intricate temporal and cell-type specific roles of cell-ECM interactions
595 in the regulation of aortic arch morphogenesis at multiple steps of its formation and
596 remodeling (Fig. 8).
597

598 **Acknowledgements** We thank Richard Hynes, Chenleng Cai, Sylvia Evans, Benoit
599 Bruneau, Heicko Lickert, and Hongkui Zeng for the gift of mouse strains, and Brianna
600 Alexander and Nathan Astrof for careful reading of the manuscript.

601

602 **Sources of Funding** This work was supported by the funding from the National Heart,
603 Lung, and Blood Institute of the NIH R01 HL103920, R01 HL134935, and R21
604 OD025323-01 to SA, and pre-doctoral fellowship F31HL150949 to AJR.

605 **Disclosures** None

606 **Supplemental Materials**
607 Expanded Materials & Methods
608 Online Figures 1 – 7

609 **Figure Legends**

610 *Figure legends are also included with the figures*

611 **Figure1. Endothelial PAA progenitors are arise in the SHF as early as E7.25.**
612 Isl1^{MerCreMer} and Mef2C-AHF-DreERT2 males were mated with the appropriate reporter
613 females (see Methods). E0.5 was considered to be noon on the day of the vaginal plug.
614 Tamoxifen was injected at specified times, embryos were dissected at E10.5, and
615 stained to detect VEGFR2 (blue), ERG (red), or tdTomato (orange). **A.** Sagittal view and
616 3D reconstruction through the left pharyngeal region. Inset- 3D reconstruction of PAAs.
617 **A1 – A2.** Sagittal optical sections through the embryo shown in **A.** Labeling efficiency
618 was quantified by calculating the ratio of the number of ERG^{+} tdTomato^{+} ECs to the
619 total number of ERG^{+} ECs in PAAs using IMARIS spot function. **B.** Highest labeling of
620 PAA endothelium occurred when tamoxifen was injected at E7.25 in Isl1^{MerCreMer} knockin
621 mice. **B1.** SHF-derived cells continute to be added the 4th PAA after E9.5. C. Peak
622 labeling of PAA ECs occurred when tamoxifen was injected at E8.0 in MEF2C-AHF-
623 DreERT2 strain. **C1.** Injection of tamoxifen at E8.5 led to a more efficient labeling of the
624 4th PAAs than the 3rd and 6th PAAs.

625 **Figure 2. Majority of PAA ECs are SHF-derived; there are differences in the**
626 **contribution of the SHF to the PAA endothelium depending on the strain used.**
627 Mef2C-AHF-Cre; ROSA^{tdTomato} embryos (35 – 37 somites) were stained with antibodies
628 to VEGFR2 (turquoise) to detect endothelial cells, tdTomato (orange) to detect SHF-
629 derived cells, and DAPI (blue) to stain cell nuclei. **A – A2.** 3D reconstructions of PAAs
630 and their connections with the dorsal aorta (dAo) and the aortic sac (Ao S). **B – B2.**

631 Sagittal optical sections to show the distribution of all SHF-derived cells in the
632 pharyngeal arches. PAAs 3 – 6 are labeled. Magnifications are the same in all panels.
633 All scale bars are 100 μm. **C.** The number of VEGFR2^{+}EGR^{+} cells in the pharyngeal
634 arches was quantified in 5 E10.5 embryos at 35 – 37 somites using IMARIS. Each dot is
635 one arch. Red line marks the median. Black lines mark quartiles. Differences among the
636 three PAA pairs are not significant, $p>0.1$ by one-way ANOVA with Tukey's correction
637 for multiple testing. **D – E.** The percentage of VEGFR2^{+}EGR^{+} cells expressing the Cre
638 reporter was determined in each PAA (orange bars). Blue bars are the percent of
639 VEGFR2^{+}EGR^{+} cells that were not labeled with the Cre reporter. **D.** The use of
640 constitutive Isl1^{Cre} strain resulted in labeling of more than 80% of ECs in the 3rd and 4th
641 PAAs. **E.** The use of Mef2C-AHF-Cre strain resulted in a significantly higher labeling of
642 the 4th PAAs than the 3rd and the 6th. The difference in the labeling efficiency of 6th
643 PAAs between the two strains was not significant, $p> 0.2$. All statistical analyses were
644 performed using one-way ANOVA with Tukey's correction for multiple testing.

645

646 **Figure 3. Formation of the 4th PAA is delayed in integrin α5$^{flox/-}$; Isl1^{Cre} mutants.**
647 Integrin α5$^{flox/+}$; Isl1^{Cre} control and α5$^{flox/-}$; Isl1^{Cre} mutant embryos were dissected at
648 different somite stages at E10.5 and stained to detect Pecam1. PAAs are numbered
649 and somite stages are indicated in the first row. **A, D, G, J.** 3D reconstructions of whole-
650 mount Pecam 1 staining (light blue). **B, E, H, K.** PAA endothelium in the 3rd, 4th and 6th
651 arches shown in the row above was surface-rendered white, green and red,
652 respectively. In addition, the plexus endothelium in the 4th arch was surface-rendered in
653 pink. **C, F, I, L.** Left side and ventral views of surface-rendered PAAs and the plexus.

654 Development of the 4th PAAs was specifically affected in the mutants (**E, F**).
655 Magnification is the same in all panels. Scale bar is 100 μm. **M.** Total number of
656 endothelial cells was quantified as described in Methods. Mutants have EC deficiency in
657 the 4th arch as 32 – 33 somites. **N.** The sizes of the 4th arches are comparable between
658 controls and mutants. **O.** EC proliferation in the PAA and the plexus in the 4th arches
659 was similar in controls (C) and mutants (M). In all plots, solid lines mark the median,
660 dashed lines mark the quartiles. Each dot marks one arch. At least 3 mutants and 3
661 controls were assayed. Statistics were evaluated using 2-tailed, unpaired Student's t
662 test with Welch's correction for unequal standard deviation between samples.

663

664 **Figure 4**. **The expression of integrin a5 in the Isl1 lineages is required for the**
665 **accrual of SHF-derived cells to the pharyngeal mesenchyme.** Control and mutant
666 embryos carrying one ROSA^{nTnG} reporter allele were dissected at E9.5 (18 – 20 somite
667 stage) and stained with DAPI and anti-GFP antibodies. Whole embryos were imaged
668 and the number of GFP$^+$ cells (SHF-derivatives) in the arch mesenchyme, splanchnic
669 mesoderm, and in the heart was quantified as described in Sup. Fig. 4. **A.** The total
670 number of SHF cells in the mesenchyme of the 1st and 2nd arches was decreased in the
671 mutants. **B.** The total number of of GFP$^+$ cells in the pharyngeal mesenchyme
672 corresponding with the future arches 3 – 6 was decreased in the mutants. The number
673 of SHF cells in heart (**C**) and the splanchnic mesoderm (**D**) was not affected. **E.** The
674 proportion of GFP$^+$ cells in the heart relative to GFP$^+$ cells in splanchnic mesoderm was
675 not affected in the mutants. **F.** The proportion of GFP$^+$ cells in the posterior pharyngeal
676 mesenchyme relative to the number of GFP$^+$ cells in splanchnic mesoderm was

677 significantly decreased in the mutants. Each dot marks one embryo, red lines mark
678 medians, dotted lines mark quartiles; p values were determined using unpaired, 2-tailed
679 Student's t tests.

680

681 **Figure 5. Recovery of EC numbers in integrin $\alpha5^{flox/-}$; Isl1$^{Cre/+}$ mutants. A.** Total EC
682 number has recovered in integrin a5$^{flox/-}$; Isl1$^{Cre/+}$ mutants by the 34th somite stage. **B.**
683 Total number of SHF-derived mesodermal cells has recovered in the pharyngeal arches
684 in integrin $\alpha5^{flox/-}$; Isl1$^{Cre/+}$ mutants by the 34th somite stage. **C.** The fraction of SHF-
685 derived ECs in pharyngeal arches is comparable among control and mutant embryos.
686 This fraction was calculated by quantifying the number of GFP^{+}ERG^{+} cells and dividing
687 by the total number of ERG^{+} cells in the entire pharyngeal arches (e.g. ECs in PAA and
688 plexus were quantified). Statistical significance was evaluated using one-way ANOVA
689 with Tukey's correction for multiple testing.

690

691 **Figure 6. Integrin α5b1 and Fn1 regulate the remodeling of EC plexus during the**
692 **formation of the 4th pharyngeal arch arteries. A.** The proportion of ECs in the 4th
693 PAAs in the mutant is significantly lower than in controls at all stages analyzed at E10.5,
694 including the stages when the EC population in the 4th pharyngeal arch has recovered in
695 the mutants; 2-tailed, unpaired Student's t test. **B – C.** Linear regression analyses
696 indicate the absence of linear correlation between the size of the 4th PAA and EC
697 number (**B**) or density (**C**). PAA size is expressed as the percentage of pharyngeal arch
698 endothelial cells in the 4th PAA in control embryos on the y-axis. **D.** Total EC number (x-

699 axis) from mutants with defective (open symbols) or unaffected 4th PAA (closed
700 symbols) were plotted against the size of the 4th PAAs, y -axis. Regression analysis
701 indicated low correlation between these properties. Circles: 32 – 33 somite embryos,
702 rhombi: 34 – 35 somite embryos, triangles: 36 – 39 somite embryos. **E.** The
703 rearrangement of the endothelial plexus into the 4th PAAs is defective in mutants
704 relative to controls with the same number of endothelial cells in the 4th arch (red boxes).
705 EC – endothelial cell(s). Controls: $\alpha5^{f/+}$; Isl1$^{Cre/+}$ and Fn1$^{f/+}$; Isl1$^{Cre/+}$ embryos; Mutants:
706 $\alpha5^{f/-}$; Isl1$^{Cre/+}$ and Fn1$^{f/-}$; Isl1$^{Cre/+}$ embryos.

707 **Figure 7. The expression of integrin α5β1 in the Isl1 lineages regulates the**
708 **differentiation of neural crest-derived cells into VSCMs at E11.5 A.** PAA perimeter
709 has recovered in size in the mutants by E11.5. **B.** Smooth muscle coverage of the left
710 4th and left 6th PAA was deficient in the mutants. **C – D**. Despite defective differentiation
711 of NC cells into VSMCs, the activation of Notch in the pharyngeal arch mesenchyme
712 was not altered in the mutants. PAAs are numbered. PAA lumens at E11.5 are derived
713 from the Isl1^{Cre} lineage (green, arrowheads in **C1** and **D1**). αSMA^{+} cells are GFP-
714 negative in Isl1^{Cre} strain (arrows in **C1-C2**). **C2 – D2**. VSMC differentiation assayed by
715 the expression of alpha smooth muscle actin (αSMA, blue) is specifically affected
716 around the 4th PAAs in the mutants (compare regions marked by the arrows in **C2** and
717 **D2**). The activation of Notch assayed by the expression of NICD is not altered in the
718 mutants with defective VSCM differentiation (arrows in **C3, C4** and **D3, D4**). **E.** Fate
719 map using TFAP2α^{IRESCre} shows the location of NC-derived cells in the pharyngeal
720 arches. Note extensive colonization of the mesenchyme between the endodermal
721 pouches (endo) by the TFAP2α^{IRESCre} lineage. **E2**. αSMA^{+} cells are GFP^{+} in

722 TFAP2$\alpha^{IRESCre}$ strain. All scale bars are 50 μm. Additional zoom-out views are in Sup.
723 Fig. 6.

724

725 **Figure 8. Cell – ECM interactions play essential roles at multiple stages during the**
726 **development of the aortic arch and its branches. A.** The expression of integrin α5β1
727 and Fn1 in the Isl1 lineages is required for the formation of the 4th PAAs. **A1**. A
728 schematic of Isl1 lineages (green) in the pharynx at E8.5 – E9.5. Green arrows indicate
729 migration of splanchnic mesoderm cells into the pharyngeal arches. Red lines signify
730 enriched localization of Fn1 protein at germ layer borders. Integrin α5β1 is expressed in
731 all cell types in the pharynx at E8.5 (Chen et al., 2015) and regulates the accrual of
732 pharyngeal mesoderm from the SHF (green arrows). **A2.** During the 10th day of mouse
733 development, integrin a5b1 and Fn1 regulate the remodeling of the plexus endothelium
734 in the 4th pharyngeal arch into the PAA. Isl1 lineages are marked in green. NC-derived
735 cells are in blue. **B.** The expression of integrin a5 in the mesoderm regulates the
736 differentiation of NC-derived cells into VSMCs. The deletion of integrin α5 in Mesp1
737 lineage, which includes the SHF, leads to defective NC-to-VSMC differentiation and
738 results in the regression of the 4th PAAs leading to IAA-B and RERSA (Liang, et al., *Dev*
739 *Biol* 2014). **C.** Fn1 becomes upregulated in NC-derived cells adjacent to the 4th PAA
740 ECs between E10.5 and E11.5 The expression of integrin α5β1 and Fn1 in the NC-
741 derived cells is required for NC-to-VSMC differentiation and the stability of the 4th PAA
742 (Wang et al, 2016). The deletion of either α5 or Fn1 in the NC (and the surface
743 ectoderm) leads to IAA-B and RERSA but does not impair PAA formation.

744

745 **Supplemental Figure 1. Delayed formation of the 4th PAAs in mutants lacking**
746 **integrin α5 or Fn1 in the Isl1 lineages. A – B.** Quantification of total endothelial cell
747 numbers in the 4th arches of controls and mutants show similar phenotypes among
748 integrin $\alpha5^{flox/-}$; Isl1$^{Cre/+}$ and Fn1$^{flox/-}$; Isl1$^{Cre/+}$ embryos. Note the recovery of endothelial
749 cell numbers at 36 – 40-somite stage. **C.** Combined data comparing endothelial
750 populations of controls and integrin $\alpha5^{flox/-}$; Isl1$^{Cre/+}$ and Fn1$^{flox/-}$; Isl1$^{Cre/+}$ mutant embryos
751 at 33 – 34-somite stages. **D.** The proportion of pharyngeal ECs in the plexus is
752 increased in the mutants relative to controls. **E.** The proportion of endothelial cells in the
753 PAA is decreased in the mutants relative to controls. Note, 7 of 16 mutants did not have
754 PAAs (0% endothelial cells in the 4th PAA).
755
756 **Supplemental Figure 2. The prevalence of cell death, as assayed by the presence**
757 **of cleaved caspase 3 or TUNEL signals, was similar in controls and mutants. A, C.**
758 Controls. **B, D.** Mutants. All scale bars are 100 μm.
759
760 **Supplemental Figure 3**. **The differentiation of SHF-derived cells into endothelial**
761 **cells is not affected by the deletion of integrin α5 in the Isl1 lineages.** Whole-mount
762 staining, confocal imaging and 3D reconstruction through the pharyngeal regions of
763 control (**A, C**) and mutant (**B, D**) embryos. **A – B.** Sagittal optical sections through E9.5
764 embryos: The majority of VEGFR2^{+} cells express GFP and ERG in the 3rd PAA and in a
765 more posterior mesenchyme (arrows) in controls and mutants. **C – D.** E10.5 embryos.
766 3D reconstruction through the pharyngeal region. Open chevrons mark the 4th PAAs.

767 Note the presence of a very thin PAA in the mutant (**D-D1**). All VERGFR2^{+} cells are
768 Pecam1^{+} in control and in the mutant with defective 4th PAA. Scale bars are 50 μm.
769
770 **Supplemental Figure 4. Quantification of SHF-derived cells in pharyngeal**
771 **mesenchyme and splanchnic mesoderm.** E9.5 Isl1$^{Cre/+}$; Rosa$^{nTnG/+}$ embryos were
772 stained with anti-GFP antibodies, cleared in BABB, and imaged through the entire
773 pharyngeal region using 25x silicone oil objective N.A. 1.05 and Nikon confocal
774 microscope. 3D reconstruction and surfacing were done using IMARIS. **A.** Pharyngeal
775 mesenchyme in the 1st and 2nd pharyngeal arches was surfaced. Dashed line marks the
776 plane of transverse optical section shown in **A1**. GFP^{+} cells within the pharyngeal
777 mesenchyme (yellow) were quantified using the spot function in IMARIS in the entire
778 volume marked by the yellow surfaces in **A. B –B4**. Splanchnic mesoderm within the
779 dorsal pericardial wall was surfaced in pink, and pharyngeal mesenchyme was surfaced
780 in yellow. **B.** Ventral view. **B1.** Right-side view. Dashed line indicates the plane of
781 section shown in **B3. B2.** A slanted, sagittal/coronal view to visualize both the
782 splanchnic mesoderm and pharyngeal mesenchyme. **B3**. GFP^{+} cells in the splanchnic
783 mesoderm (pink) and in the posterior pharyngeal mesenchyme (yellow) were quantified
784 using the spot function in IMARIS throughout the entire volume shown in **B**.
785
786 **Supplemental Figure 5**. **Step-wise changes in the configuration of the 4th arch**
787 **endothelium on the 10th day of mouse embryonic development.** Control embryos
788 were stained using antibody to Pecam1. Endothelial cells in the 4th pharyngeal arch
789 were surface-rendered yellow using IMARIS. First row, 30-somite stage. Endothelium in

790 the 4th arch is in the form of a plexus of small blood vessels. Second row 33-somite
791 embryo. A small PAA is seen forming. Red starts mark spaces amidst the
792 interconnected plexus vessels and the small PAA. Third row, 33-somite stage. A large
793 PAA is seen with connecting plexus vessels. Spaces (marked by the red stars) are still
794 seen. Fourth row – 36 – 40 – somite stage. A large PAA is present in the 4th arch by the
795 evening of the 10th day. DA – dorsal aorta. PAAs are numbers. All scale bars are 50 μm.
796
797 **Supplemental Figure 6. The expression of integrin α5β1 in the Isl1 lineages**
798 **regulates the differentiation of neural crest-derived cells into VSCMs at E11.5**
799 Activation of Notch in the pharyngeal arch mesenchyme is not altered in the mutants.
800 Coronal section through the pharyngeal regions of Control (**A**) and Mutant (**B**) embryos
801 were stained to detect green fluorescent protein (GFP, green) marks the Isl1 lineages;
802 Notch intracellular domain (NICD, orange) is used as the readout of active Notch
803 signaling; and a smooth muscle actin (αSMA, blue) marks smooth muscle cells. PAAs
804 are numbered. The magnification is the same in all panels.
805
806 **Supplemental Figure 7. PAA formation is not affected when integrin α5 is ablated**
807 **using Sox17$^{2A\text{-}iCre}$ knock-in strain.** Whole-mount pictures were taken following India
808 Ink injections into the hearts of controls and mutants isolated at E10.5. Magnification is
809 the same in all panels.
810

811 **References**

812 1. Stoller JZ and Epstein JA. Cardiac neural crest. *Semin Cell Dev Biol*.
813 2005;16:704-15.

814 2. Schreiber C, Mazzitelli D, Haehnel JC, Lorenz HP and Meisner H. The
815 interrupted aortic arch: an overview after 20 years of surgical treatment. *Eur J*
816 *Cardiothorac Surg*. 1997;12:466-9; discussion 469-70.

817 3. Kellenberger CJ. Aortic arch malformations. *Pediatr Radiol*. 2010;40:876-84.

818 4. Psillas G, Kekes G, Constantinidis J, Triaridis S and Vital V. Subclavian steal
819 syndrome: neurotological manifestations. *Acta Otorhinolaryngol Ital*. 2007;27:33-7.

820 5. Kirby ML. *Cardiac Development*. New York: Oxford University Press; 2007.

821 6. Moon A. Mouse models of congenital cardiovascular disease. *Curr Top Dev Biol*.
822 2008;84:171-248.

823 7. Nagelberg D, Wang J, Su R, Torres-Vazquez J, Targoff KL, Poss KD and Knaut
824 H. Origin, Specification, and Plasticity of the Great Vessels of the Heart. *Curr Biol*.
825 2015;25:2099-110.

826 8. Paffett-Lugassy N, Singh R, Nevis KR, Guner-Ataman B, O'Loughlin E, Jahangiri
827 L, Harvey RP, Burns CG and Burns CE. Heart field origin of great vessel precursors
828 relies on nkx2.5-mediated vasculogenesis. *Nat Cell Biol*. 2013;15:1362-9.

829 9. Wang X, Chen D, Chen K, Jubran A, Ramirez A and Astrof S. Endothelium in the
830 pharyngeal arches 3, 4 and 6 is derived from the second heart field. *Dev Biol*.
831 2017;421:108-117.

832 10. Li P, Pashmforoush M and Sucov HM. Mesodermal retinoic acid signaling
833 regulates endothelial cell coalescence in caudal pharyngeal arch artery vasculogenesis.
834 *Dev Biol*. 2012;361:116-24.

835 11. Bremer JL. The development of the aorta and aortic arches in rabbits. *American*
836 *Journal of Anatomy*. 1912;13:111-128.

837 12. DeRuiter MC, Poelmann RE, Mentink MM, Vaniperen L and Gittenberger-De
838 Groot AC. Early formation of the vascular system in quail embryos. *Anat Rec*.
839 1993;235:261-74.

840 13. Abrial M, Paffett-Lugassy N, Jeffrey S, Jordan D, O'Loughlin E, Frederick CJ,
841 3rd, Burns CG and Burns CE. TGF-beta Signaling Is Necessary and Sufficient for
842 Pharyngeal Arch Artery Angioblast Formation. *Cell Rep*. 2017;20:973-983.

843 14. Guner-Ataman B, Paffett-Lugassy N, Adams MS, Nevis KR, Jahangiri L,
844 Obregon P, Kikuchi K, Poss KD, Burns CE and Burns CG. Zebrafish second heart field
845 development relies on progenitor specification in anterior lateral plate mesoderm and
846 nkx2.5 function. *Development*. 2013;140:1353-63.

847 15. Guner-Ataman B, Gonzalez-Rosa JM, Shah HN, Butty VL, Jeffrey S, Abrial M,
848 Boyer LA, Burns CG and Burns CE. Failed Progenitor Specification Underlies the
849 Cardiopharyngeal Phenotypes in a Zebrafish Model of 22q11.2 Deletion Syndrome. *Cell*
850 *Rep*. 2018;24:1342-1354 e5.

851 16. Holowiecki A, Linstrum K, Ravisankar P, Chetal K, Salomonis N and Waxman
852 JS. Pbx4 limits heart size and fosters arch artery formation through partitioning second
853 heart field progenitors and restricting proliferation. *Development*. 2020.

854 17. Gittenberger-de Groot AC, DeRuiter MC, Bergwerff M and Poelmann RE.
855 Smooth muscle cell origin and its relation to heterogeneity in development and disease.
856 *Arterioscler Thromb Vasc Biol*. 1999;19:1589-94.

857 18. Bockman DE, Redmond ME, Waldo K, Davis H and Kirby ML. Effect of neural
858 crest ablation on development of the heart and arch arteries in the chick. *The American*
859 *journal of anatomy*. 1987;180:332-41.

860 19. Hutson MR and Kirby ML. Model systems for the study of heart development and
861 disease. Cardiac neural crest and conotruncal malformations. *Semin Cell Dev Biol*.
862 2007;18:101-10.

863 20. Hutson MR, Sackey FN, Lunney K and Kirby ML. Blocking hedgehog signaling
864 after ablation of the dorsal neural tube allows regeneration of the cardiac neural crest
865 and rescue of outflow tract septation. *Dev Biol*. 2009;335:367-73.

866 21. Rosenquist TH, Kirby ML and van Mierop LH. Solitary aortic arch artery. A result
867 of surgical ablation of cardiac neural crest and nodose placode in the avian embryo.
868 *Circulation*. 1989;80:1469-75.

869 22. Keyte A and Hutson MR. The neural crest in cardiac congenital anomalies.
870 *Differentiation; research in biological diversity*. 2012;84:25-40.

871 23. Coles EG, Gammill LS, Miner JH and Bronner-Fraser M. Abnormalities in neural
872 crest cell migration in laminin alpha5 mutant mice. *Dev Biol*. 2006;289:218-28.

873 24. Cooley MA, Kern CB, Fresco VM, Wessels A, Thompson RP, McQuinn TC, Twal
874 WO, Mjaatvedt CH, Drake CJ and Argraves WS. Fibulin-1 is required for
875 morphogenesis of neural crest-derived structures. *Dev Biol*. 2008;319:336-45.

876 25. Rydeen AB and Waxman JS. Cyp26 Enzymes Facilitate Second Heart Field
877 Progenitor Addition and Maintenance of Ventricular Integrity. *PLoS Biol*.
878 2016;14:e2000504.

879 26. Wickstrom SA, Radovanac K and Fassler R. Genetic analyses of integrin
880 signaling. *Cold Spring Harb Perspect Biol*. 2011;3.

881 27. Astrof S. Interactions between neural crest-derived cells and extracellular
882 microenvironment during cardiovascular development. In: D. W. Desimone and R. P.
883 Mecham, eds. *Extracellular Matrix in Development* Berlin: Springer Verlag; 2013: 105-
884 131.

885 28. Mittal A, Pulina M, Hou SY and Astrof S. Fibronectin and integrin alpha 5 play
886 essential roles in the development of the cardiac neural crest. *Mech Dev*. 2010;127:472-
887 84.

888 29. Chen D, Wang X, Liang D, Gordon J, Mittal A, Manley N, Degenhardt K and
889 Astrof S. Fibronectin signals through integrin alpha5beta1 to regulate cardiovascular
890 development in a cell type-specific manner. *Dev Biol*. 2015;407:195-210.

891 30. Wang X and Astrof S. Isolation of Mouse Cardiac Neural Crest Cells and Their
892 Differentiation into Smooth Muscle Cells. *Bio Protoc*. 2017;7.

893 31. Wang X and Astrof S. Neural crest cell-autonomous roles of fibronectin in
894 cardiovascular development. *Development*. 2016;143:88-100.

895 32. Humphries JD, Byron A and Humphries MJ. Integrin ligands at a glance. *J Cell*
896 *Sci*. 2006;119:3901-3.

897 33. Hynes RO and Naba A. Overview of the matrisome--an inventory of extracellular
898 matrix constituents and functions. *Cold Spring Harbor perspectives in biology*.
899 2012;4:a004903.

900 34. Pulina M, Liang D and Astrof S. Shape and position of the node and notochord
901 along the bilateral plane of symmetry are regulated by cell-extracellular matrix
902 interactions. *Biology open*. 2014;3:583-90.

903 35. George EL, Baldwin HS and Hynes RO. Fibronectins are essential for heart and
904 blood vessel morphogenesis but are dispensable for initial specification of precursor
905 cells. *Blood*. 1997;90:3073-81.

906 36. George EL, Georges-Labouesse EN, Patel-King RS, Rayburn H and Hynes RO.
907 Defects in mesoderm, neural tube and vascular development in mouse embryos lacking
908 fibronectin. *Development*. 1993;119:1079-91.

909 37. Georges-Labouesse EN, George EL, Rayburn H and Hynes RO. Mesodermal
910 development in mouse embryos mutant for fibronectin. *Dev Dyn*. 1996;207:145-56.

911 38. Pulina MV, Hou SY, Mittal A, Julich D, Whittaker CA, Holley SA, Hynes RO and
912 Astrof S. Essential roles of fibronectin in the development of the left-right embryonic
913 body plan. *Dev Biol*. 2011;354:208-20.

914 39. Yang JT, Bader BL, Kreidberg JA, Ullman-Cullere M, Trevithick JE and Hynes
915 RO. Overlapping and independent functions of fibronectin receptor integrins in early
916 mesodermal development. *Dev Biol*. 1999;215:264-77.

917 40. Yang JT, Rayburn H and Hynes RO. Embryonic mesodermal defects in alpha 5
918 integrin-deficient mice. *Development*. 1993;119:1093-105.

919 41. Mittal A, Pulina M, Hou S and Astrof S. Fibronectin and integrin alpha 5 play
920 requisite roles in cardiac morphogenesis. *Dev Biol*. 2013;381:73-82.

921 42. Sun Y, Liang X, Najafi N, Cass M, Lin L, Cai CL, Chen J and Evans SM. Islet 1 is
922 expressed in distinct cardiovascular lineages, including pacemaker and coronary
923 vascular cells. *Dev Biol*. 2007;304:286-96.

924 43. Devine WP, Wythe JD, George M, Koshiba-Takeuchi K and Bruneau BG. Early
925 patterning and specification of cardiac progenitors in gastrulating mesoderm. *eLife*.
926 2014;3.

927 44. Ramirez A and Astrof S. Visualization and Analysis of Pharyngeal Arch Arteries
928 using Whole-mount Immunohistochemistry and 3D Reconstruction. *J Vis Exp*.
929 2020;157:e60797.

930 45. Fish JE, Cantu Gutierrez M, Dang LT, Khyzha N, Chen Z, Veitch S, Cheng HS,
931 Khor M, Antounians L, Njock MS, Boudreau E, Herman AM, Rhyner AM, Ruiz OE,
932 Eisenhoffer GT, Medina-Rivera A, Wilson MD and Wythe JD. Dynamic regulation of
933 VEGF-inducible genes by an ERK/ERG/p300 transcriptional network. *Development*.
934 2017;144:2428-2444.

935 46. Jia G, Preussner J, Chen X, Guenther S, Yuan X, Yekelchyk M, Kuenne C,
936 Looso M, Zhou Y, Teichmann S and Braun T. Single cell RNA-seq and ATAC-seq
937 analysis of cardiac progenitor cell transition states and lineage settlement. *Nat*
938 *Commun*. 2018;9:4877.

939 47. Verzi MP, McCulley DJ, De Val S, Dodou E and Black BL. The right ventricle,
940 outflow tract, and ventricular septum comprise a restricted expression domain within the
941 secondary/anterior heart field. *Dev Biol*. 2005;287:134-45.

942 48. Dodou E, Verzi MP, Anderson JP, Xu SM and Black BL. Mef2c is a direct
943 transcriptional target of ISL1 and GATA factors in the anterior heart field during mouse
944 embryonic development. *Development*. 2004;131:3931-42.

945 49. Papangeli I and Scambler PJ. Tbx1 genetically interacts with the transforming
946 growth factor-beta/bone morphogenetic protein inhibitor Smad7 during great vessel
947 remodeling. *Circ Res*. 2013;112:90-102.

948 50. Lindsay EA and Baldini A. Recovery from arterial growth delay reduces
949 penetrance of cardiovascular defects in mice deleted for the DiGeorge syndrome
950 region. *Human molecular genetics*. 2001;10:997-1002.

951 51. Waldo KL, Kumiski D and Kirby ML. Cardiac neural crest is essential for the
952 persistence rather than the formation of an arch artery. *Dev Dyn*. 1996;205:281-92.

953 52. High FA, Zhang M, Proweller A, Tu L, Parmacek MS, Pear WS and Epstein JA.
954 An essential role for Notch in neural crest during cardiovascular development and
955 smooth muscle differentiation. *J Clin Invest*. 2007;117:353-63.

956 53. High FA, Jain R, Stoller JZ, Antonucci NB, Lu MM, Loomes KM, Kaestner KH,
957 Pear WS and Epstein JA. Murine Jagged1/Notch signaling in the second heart field
958 orchestrates Fgf8 expression and tissue-tissue interactions during outflow tract
959 development. *J Clin Invest*. 2009;119:1986-96.

960 54. High FA, Lu MM, Pear WS, Loomes KM, Kaestner KH and Epstein JA.
961 Endothelial expression of the Notch ligand Jagged1 is required for vascular smooth
962 muscle development. *Proceedings of the National Academy of Sciences %R*
963 *101073/pnas0709663105*. 2008;105:1955-1959.

964 55. Manderfield LJ, Aghajanian H, Engleka KA, Lim LY, Lui F, Jain R, Li L, Olson EN
965 and Epstein JA. Hippo signaling is required for Notch-dependent smooth muscle
966 differentiation of neural crest. *Development*. 2015.

967 56. Manderfield LJ, High FA, Engleka KA, Liu F, Li L, Rentschler S and Epstein JA.
968 Notch activation of Jagged1 contributes to the assembly of the arterial wall. *Circulation*.
969 2012;125:314-23.

970 57. Hellstrom M, Gerhardt H, Kalen M, Li X, Eriksson U, Wolburg H and Betsholtz C.
971 Lack of pericytes leads to endothelial hyperplasia and abnormal vascular
972 morphogenesis. *J Cell Biol*. 2001;153:543-53.

973 58. Jiang X, Rowitch DH, Soriano P, McMahon AP and Sucov HM. Fate of the
974 mammalian cardiac neural crest. *Development*. 2000;127:1607-1616.

975 59. Liang D, Wang X, Mittal A, Dhiman S, Hou SY, Degenhardt K and Astrof S.
976 Mesodermal expression of integrin alpha5beta1 regulates neural crest development and
977 cardiovascular morphogenesis. *Dev Biol*. 2014;395:232–244.

978 60. Engleka KA, Manderfield LJ, Brust RD, Li L, Cohen A, Dymecki SM and Epstein
979 JA. Islet1 derivatives in the heart are of both neural crest and second heart field origin.
980 *Circ Res*. 2012;110:922-6.

981 61. van der Flier A, Badu-Nkansah K, Whittaker CA, Crowley D, Bronson RT, Lacy-
982 Hulbert A and Hynes RO. Endothelial alpha5 and alphav integrins cooperate in
983 remodeling of the vasculature during development. *Development*. 2010;137:2439-49.

984 62. Engert S, Liao WP, Burtscher I and Lickert H. Sox17-2A-iCre: a knock-in mouse
985 line expressing Cre recombinase in endoderm and vascular endothelial cells. *Genesis*.
986 2009;47:603-10.

987 63. Calmont A, Ivins S, Van Bueren KL, Papangeli I, Kyriakopoulou V, Andrews WD,
988 Martin JF, Moon AM, Illingworth EA, Basson MA and Scambler PJ. Tbx1 controls
989 cardiac neural crest cell migration during arch artery development by regulating Gbx2
990 expression in the pharyngeal ectoderm. *Development*. 2009;136:3173-83.

991 64. Gitler AD, Lu MM and Epstein JA. PlexinD1 and semaphorin signaling are
992 required in endothelial cells for cardiovascular development. *Dev Cell*. 2004;7:107-16.

993 65. Merscher S, Funke B, Epstein JA, Heyer J, Puech A, Lu MM, Xavier RJ, Demay
994 MB, Russell RG, Factor S, Tokooya K, Jore BS, Lopez M, Pandita RK, Lia M, Carrion
995 D, Xu H, Schorle H, Kobler JB, Scambler P, Wynshaw-Boris A, Skoultchi AI, Morrow BE
996 and Kucherlapati R. TBX1 is responsible for cardiovascular defects in velo-cardio-
997 facial/DiGeorge syndrome. *Cell*. 2001;104:619-29.

998 66. Phillips HM, Stothard CA, Shaikh Qureshi WM, Kousa AI, Briones-Leon JA,
999 Khasawneh RR, O'Loughlin C, Sanders R, Mazzotta S, Dodds R, Seidel K, Bates T,

1000 Nakatomi M, Cockell SJ, Schneider JE, Mohun TJ, Maehr R, Kist R, Peters H and
1001 Bamforth SD. Pax9 is required for cardiovascular development and interacts with Tbx1
1002 in the pharyngeal endoderm to control 4th pharyngeal arch artery morphogenesis.
1003 *Development*. 2019;146.

1004 67. Macatee TL, Hammond BP, Arenkiel BR, Francis L, Frank DU and Moon AM.
1005 Ablation of specific expression domains reveals discrete functions of ectoderm- and
1006 endoderm-derived FGF8 during cardiovascular and pharyngeal development.
1007 *Development*. 2003;130:6361-74.

1008 68. Cai CL, Liang X, Shi Y, Chu PH, Pfaff SL, Chen J and Evans S. Isl1 identifies a
1009 cardiac progenitor population that proliferates prior to differentiation and contributes a
1010 majority of cells to the heart. *Dev Cell*. 2003;5:877-89.

1011 69. Baldini A, Fulcoli FG and Illingworth E. Tbx1: Transcriptional and Developmental
1012 Functions. *Current topics in developmental biology*. 2017;122:223-243.

1013 70. Graham A, Okabe M and Quinlan R. The role of the endoderm in the
1014 development and evolution of the pharyngeal arches. *J Anat*. 2005;207:479-87.

1015 71. Alfano D, Altomonte A, Cortes C, Bilio M, Kelly RG and Baldini A. Tbx1 regulates
1016 extracellular matrix-cell interactions in the second heart field. *Human molecular*
1017 *genetics*. 2019;28:2295-2308.

1018 72. Francou A, Saint-Michel E, Mesbah K and Kelly RG. TBX1 regulates epithelial
1019 polarity and dynamic basal filopodia in the second heart field. *Development*.
1020 2014;141:4320-31.

1021 73. van Bueren KL, Papangeli I, Rochais F, Pearce K, Roberts C, Calmont A,
1022 Szumska D, Kelly RG, Bhattacharya S and Scambler PJ. Hes1 expression is reduced in
1023 Tbx1 null cells and is required for the development of structures affected in 22q11
1024 deletion syndrome. *Dev Biol*. 2010;340:369-80.

1025 74. Aghajanian H, Choi C, Ho VC, Gupta M, Singh MK and Epstein JA. Semaphorin
1026 3d and semaphorin 3e direct endothelial motility through distinct molecular signaling
1027 pathways. *J Biol Chem*. 2014;289:17971-9.

1028 75. Cohen ED, Wang Z, Lepore JJ, Lu MM, Taketo MM, Epstein DJ and Morrisey
1029 EE. Wnt/beta-catenin signaling promotes expansion of Isl-1-positive cardiac progenitor
1030 cells through regulation of FGF signaling. *J Clin Invest*. 2007;117:1794-804.

1031 76. Degenhardt K, Singh MK, Aghajanian H, Massera D, Wang Q, Li J, Li L, Choi C,
1032 Yzaguirre AD, Francey LJ, Gallant E, Krantz ID, Gruber PJ and Epstein JA. Semaphorin

1033 3d signaling defects are associated with anomalous pulmonary venous connections.
1034 *Nat Med*. 2013;19:760-5.

1035 77. Frank DU, Fotheringham LK, Brewer JA, Muglia LJ, Tristani-Firouzi M, Capecchi
1036 MR and Moon AM. An Fgf8 mouse mutant phenocopies human 22q11 deletion
1037 syndrome. *Development*. 2002;129:4591-603.

1038 78. Park EJ, Ogden LA, Talbot A, Evans S, Cai CL, Black BL, Frank DU and Moon
1039 AM. Required, tissue-specific roles for Fgf8 in outflow tract formation and remodeling.
1040 *Development*. 2006;133:2419-33.

1041 79. Park EJ, Watanabe Y, Smyth G, Miyagawa-Tomita S, Meyers E, Klingensmith J,
1042 Camenisch T, Buckingham M and Moon AM. An FGF autocrine loop initiated in second
1043 heart field mesoderm regulates morphogenesis at the arterial pole of the heart.
1044 *Development*. 2008;135:3599-610.

1045 80. Watanabe Y, Miyagawa-Tomita S, Vincent SD, Kelly RG, Moon AM and
1046 Buckingham ME. Role of mesodermal FGF8 and FGF10 overlaps in the development of
1047 the arterial pole of the heart and pharyngeal arch arteries. *Circ Res*. 2010;106:495-503.

1048 81. Stalmans I, Lambrechts D, De Smet F, Jansen S, Wang J, Maity S, Kneer P, von
1049 der Ohe M, Swillen A, Maes C, Gewillig M, Molin DG, Hellings P, Boetel T, Haardt M,
1050 Compernolle V, Dewerchin M, Plaisance S, Vlietinck R, Emanuel B, Gittenberger-de
1051 Groot AC, Scambler P, Morrow B, Driscol DA, Moons L, Esguerra CV, Carmeliet G,
1052 Behn-Krappa A, Devriendt K, Collen D, Conway SJ and Carmeliet P. VEGF: a modifier
1053 of the del22q11 (DiGeorge) syndrome? *Nat Med*. 2003;9:173-82.

1054 82. Oh J, Richardson JA and Olson EN. Requirement of myocardin-related
1055 transcription factor-B for remodeling of branchial arch arteries and smooth muscle
1056 differentiation. *Proc Natl Acad Sci U S A*. 2005;102:15122-7.

1057 83. Hellstrom M, Kalen M, Lindahl P, Abramsson A and Betsholtz C. Role of PDGF-B
1058 and PDGFR-beta in recruitment of vascular smooth muscle cells and pericytes during
1059 embryonic blood vessel formation in the mouse. *Development*. 1999;126:3047-55.

1060 84. Scambler PJ. The 22q11 deletion syndromes. *Human molecular genetics*.
1061 2000;9:2421-6.

1062 85. Momma K. Cardiovascular anomalies associated with chromosome 22q11.2
1063 deletion syndrome. *Am J Cardiol*. 2010;105:1617-24.

1064 86. Lindsay EA, Vitelli F, Su H, Morishima M, Huynh T, Pramparo T, Jurecic V,
1065 Ogunrinu G, Sutherland HF, Scambler PJ, Bradley A and Baldini A. Tbx1

1066 haploinsufficieny in the DiGeorge syndrome region causes aortic arch defects in mice.
1067 *Nature*. 2001;410:97-101.

1068 87. Jerome LA and Papaioannou VE. DiGeorge syndrome phenotype in mice mutant
1069 for the T-box gene, Tbx1. *Nat Genet*. 2001;27:286-91.
1070

FIGURE 1

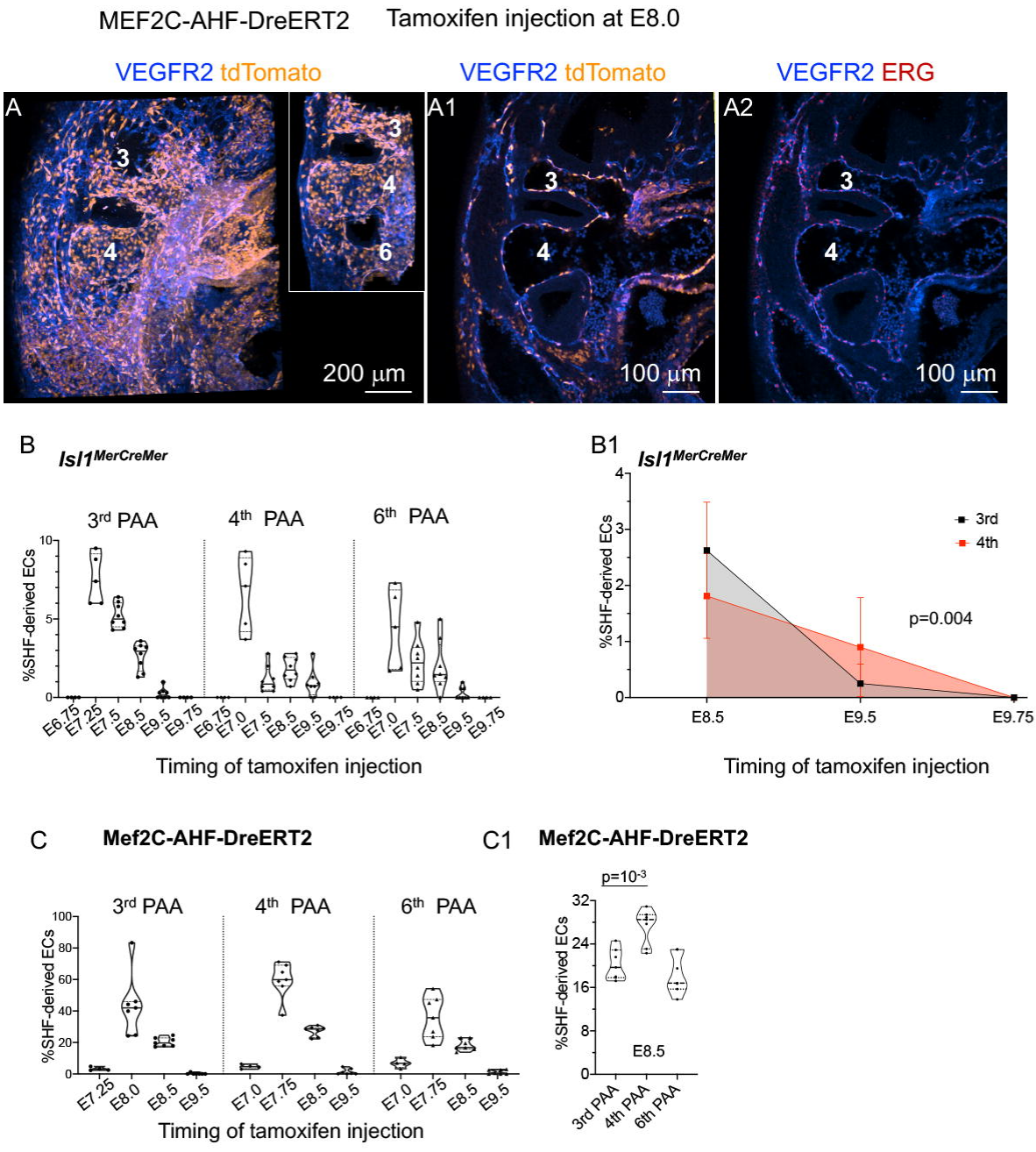

Figure1. Endothelial PAA progenitors are present in the second heart field as early as E7.25. Isl1^{MerCreMer} and Mef2C-AHF-DreERT2 males were mated with the appropriate reporter females (see Methods). E0.5 was considered to be noon on the day of the vaginal plug. Tamoxifen was injected at specified times, embryos were dissected at E10.5, and stained to detect VEGFR2 (blue), ERG (red), or tdTomato (orange). **A.** Sagittal view and 3D reconstruction through the left pharyngeal region. Inset- 3D reconstruction of PAAs. **A1 – A2.** Sagittal optical sections through the embryo shown in **A.** Labeling efficiency was quantified by calculating the ratio of the number of ERG$^+$ tdTomato$^+$ ECs to the total number of ERG$^+$ ECs in PAAs using IMARIS spot function. **B.** Highest labeling of PAA endothelium occurred when tamoxifen was injected at E7.25 in Isl1^{MerCreMer} knockin mice. **B1.** SHF-derived cells continute to be added the 4th PAA after E9.5. **C.** Peak labeling of PAA ECs occurred when tamoxifen was injected at E8.0 in MEF2C-AHF-DreERT2 strain. **C1.** Injection of tamoxifen at E8.5 led to a more efficient labeling of the 4th PAAs than the 3rd and 6th PAAs.

FIGURE 2

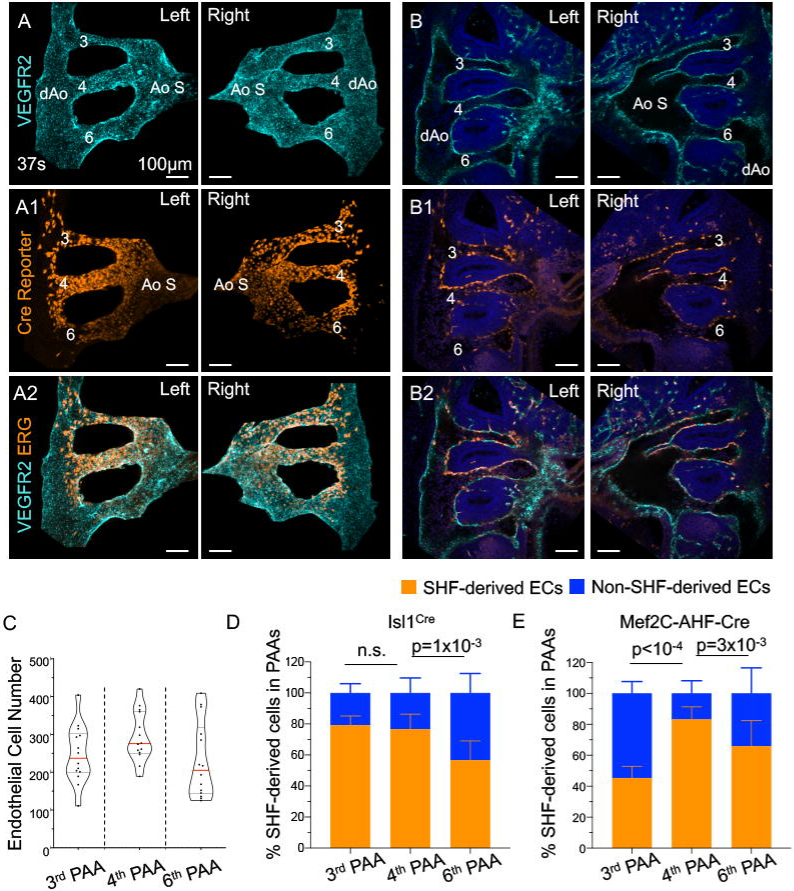

Figure 2. Majority of PAA ECs are SHF-derived; there are differences in the contribution of the SHF to the PAA endothelium depending on the strain used. Mef2C-AHF-Cre; ROSA^{tdTomato} embryos (35 – 37 somites) were stained with antibodies to VEGFR2 (turquoise) to detect endothelial cells, tdTomato (orange) to detect SHF-derived cells, and DAPI (blue) to stain cell nuclei. **A – A2.** 3D reconstructions of PAAs and their connections with the dorsal aorta (dAo) and the aortic sac (Ao S). **B – B2.** Sagittal optical sections to show the distribution of all SHF-derived cells in the pharyngeal arches. PAAs 3 – 6 are labeled. Magnifications are the same in all panels. All scale bars are 100 µm. **C.** The number of VEGFR2$^+$EGR$^+$ cells in the pharyngeal arches was quantified in 5 E10.5 embryos at 35 – 37 somites using IMARIS. Each dot is one arch. Red line marks the median. Black lines mark quartiles. Differences among the three PAA pairs are not significant, p>0.1 by one-way ANOVA with Tukey's correction for multiple testing. **D – E.** The percentage of VEGFR2$^+$EGR$^+$ cells expressing the Cre reporter was determined in each PAA (orange bars). Blue bars are the percent of VEGFR2$^+$EGR$^+$ cells that were not labeled with the Cre reporter. **D.** The use of constitutive Isl1^{Cre} strain resulted in labeling of more than 80% of ECs in the 3rd and 4th PAAs. **E.** The use of Mef2C-AHF-Cre strain resulted in a significantly higher labeling of the 4th PAAs than the 3rd and the 6th. The difference in the labeling efficiency of 6th PAAs between the two strains was not significant, p> 0.2. All statistical analyses were performed using one-way ANOVA with Tukey's correction for multiple testing.

FIGURE 3

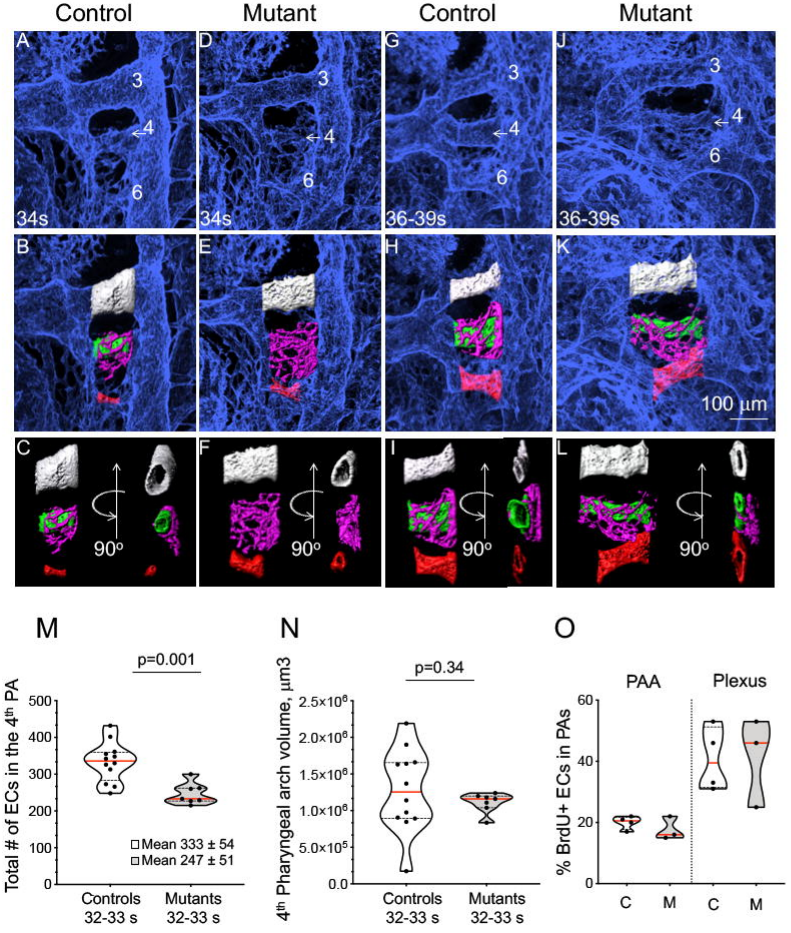

Figure 3. Formation of the 4th PAA is delayed in integrin α5$^{flox/-}$; Isl1^{Cre} mutants. α5$^{flox/+}$; Isl1^{Cre} control and α5$^{flox/-}$; Isl1^{Cre} mutant embryos were dissected at different somite stages at E10.5 and stained to detect Pecam1. PAAs are numbered and somite stages are indicated in the first row. **A, D, G, J.** 3D reconstructions of whole-mount Pecam 1 staining (light blue). **B, E, H, K.** PAA endothelium in the 3rd, 4th and 6th arches shown in the row above was surface-rendered white, green and red, respectively. In addition, the plexus endothelium in the 4th arch was surface-rendered in pink. **C, F, I, L.** Left side and ventral views of surface-rendered PAAs and the plexus. Development of the 4th PAAs was specifically affected in the mutants (**E, F**). Magnification is the same in all panels. Scale bar is 100 µm. **M**. Total number of endothelial cells was quantified as described in Methods. Mutants have EC deficiency in the 4th arch as 32 – 33 somites. **N.** The sizes of the 4th arches are comparable between controls and mutants. **O.** EC proliferation in the PAA and plexus in the 4th arches was similar in controls (C) and mutants (M). In all plots, solid lines mark the median, dashed lines mark the quartiles. Each dot marks one arch. At least 3 mutants and 3 controls were assayed. Statistics were evaluated using 2-tailed, unpaired Student's t test with Welch's correction for unequal standard deviation between samples.

FIGURE 4

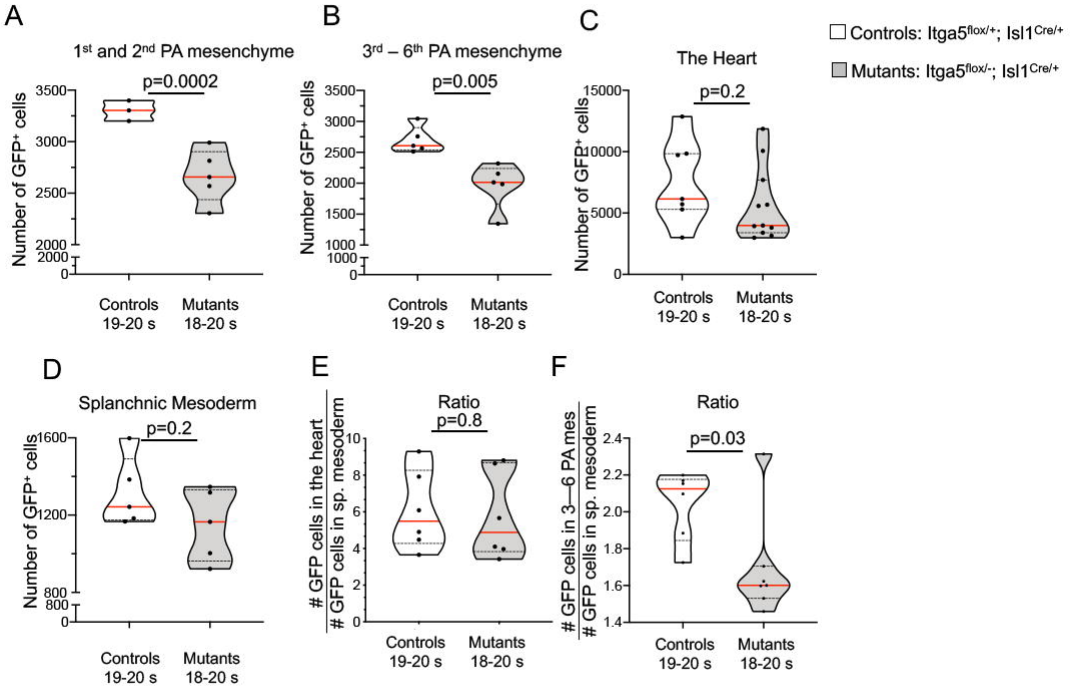

Figure 4. The expression of integrin α5 in the Isl1 lineages is required for the accrual of SHF-derived cells to the pharyngeal mesenchyme. Control and mutant embryos carrying one ROSA^{nTnG} reporter allele were dissected at E9.5 (18 – 20 somite stage) and stained with DAPI and anti-GFP antibodies. Whole embryos were imaged and the number of GFP$^+$ cells (SHF-derivatives) in the arch mesenchyme, splanchnic mesoderm, and in the heart was quantified as described in Sup. Fig. 4. **A.** The total number of SHF cells in the mesenchyme of the 1st and 2nd arches was decreased in the mutants. **B.** The total number of of GFP$^+$ cells in the pharyngeal mesenchyme corresponding with the future arches 3 – 6 was decreased in the mutants. The number of SHF cells in heart (**C**) and the splanchnic mesoderm (**D**) was not affected. **E.** The proportion of GFP$^+$ cells in the heart relative to GFP$^+$ cells in splanchnic mesoderm was not affected in the mutants. **F.** The proportion of GFP$^+$ cells in the posterior pharyngeal mesenchyme relative to the number of GFP$^+$ cells in splanchnic mesoderm was significantly decreased in the mutants. Each dot marks one embryo, red lines mark medians, dotted lines mark quartiles; p values were determined using unpaired, 2-tailed Student's t tests.

FIGURE 5

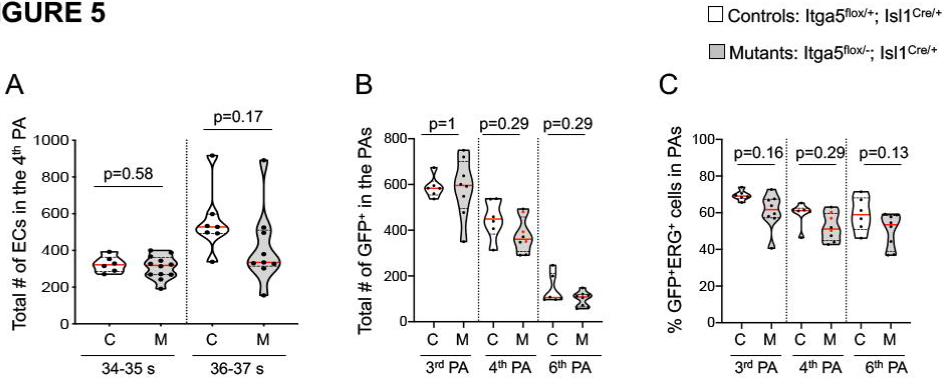

Figure 5. **Recovery of EC numbers in integrin $\alpha5^{flox/-}$; $Isl1^{Cre/+}$ mutants. A.** Total EC number has recovered in integrin $\alpha5^{flox/-}$; $Isl1^{Cre/+}$ mutants by the 34th somite stage. **B.** Total number of SHF-derived mesodermal cells has recovered in the pharyngeal arches in integrin $\alpha5^{flox/-}$; $Isl1^{Cre/+}$ mutants by the 34th somite stage. **C.** The fraction of SHF-derived ECs in pharyngeal arches is comparable among control and mutant embryos. This fraction was calculated by quantifying the number of GFP^+ERG^+ cells and dividing by the total number of ERG^+ cells in the entire pharyngeal arches (e.g. ECs in PAA and plexus were quantified). Statistical significance was evaluated using one-way ANOVA with Tukey's correction for multiple testing.

FIGURE 6

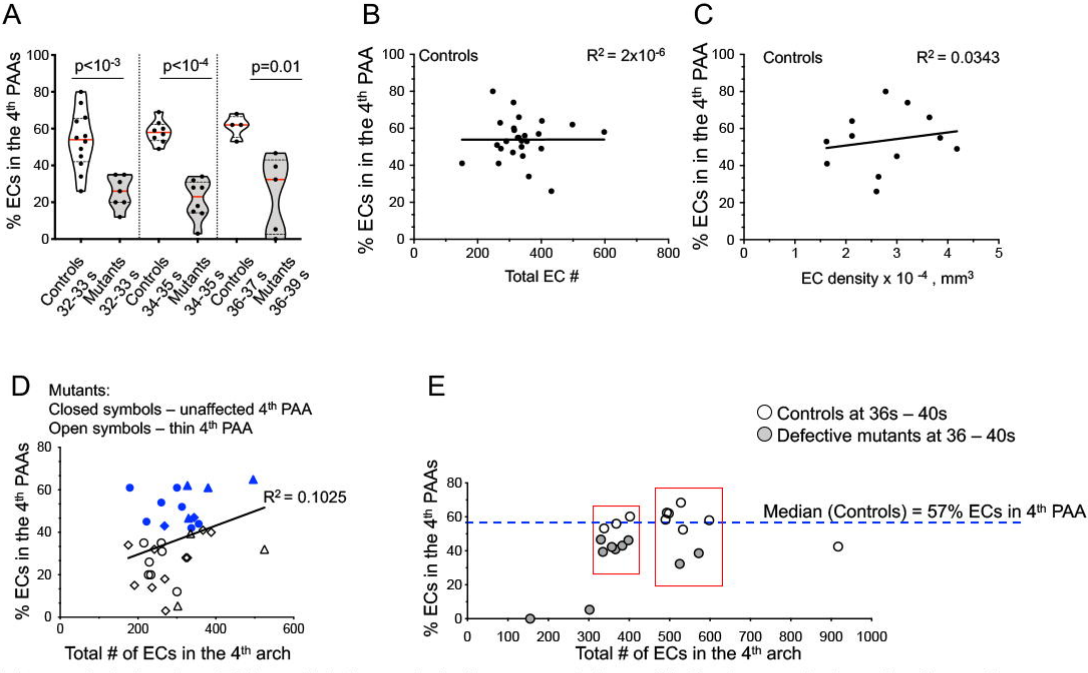

Figure 6. Integrin α5β1 and Fn1 regulate the remodeling of EC plexus during the formation of the 4th pharyngeal arch arteries. A. The proportion of ECs in the 4th PAAs in the mutant is significantly lower than in controls at all stages analyzed at E10.5, including the stages when the EC population in the 4th pharyngeal arch has recovered in the mutants; 2-tailed, unpaired Student's t test. **B – C.** Linear regression analyses indicate the absence of linear correlation between the size of the 4th PAA and EC number (**B**) or density (**C**). PAA size is expressed as the percentage of pharyngeal arch endothelial cells in the 4th PAA in control embryos on the y-axis. **D.** Total EC number (x-axis) from mutants with defective (open symbols) or unaffected 4th PAA (closed symbols) were plotted against the size of the 4th PAAs, y -axis. Regression analysis indicated low correlation between these properties. Circles: 32 – 33 somite embryos, rhombi: 34 – 35 somite embryos, triangles: 36 – 39 somite embryos. **E.** The rearrangement of the endothelial plexus into the 4th PAAs is defective in mutants relative to controls with the same number of endothelial cells in the 4th arch (red boxes). EC – endothelial cell(s). Controls: $\alpha5^{f/+}$; $Isl1^{Cre/+}$ and $Fn1^{f/+}$; $Isl1^{Cre/+}$ embryos; Mutants: $\alpha5^{f/-}$; $Isl1^{Cre/+}$ and $Fn1^{f/-}$; $Isl1^{Cre/+}$ embryos.

FIGURE 7

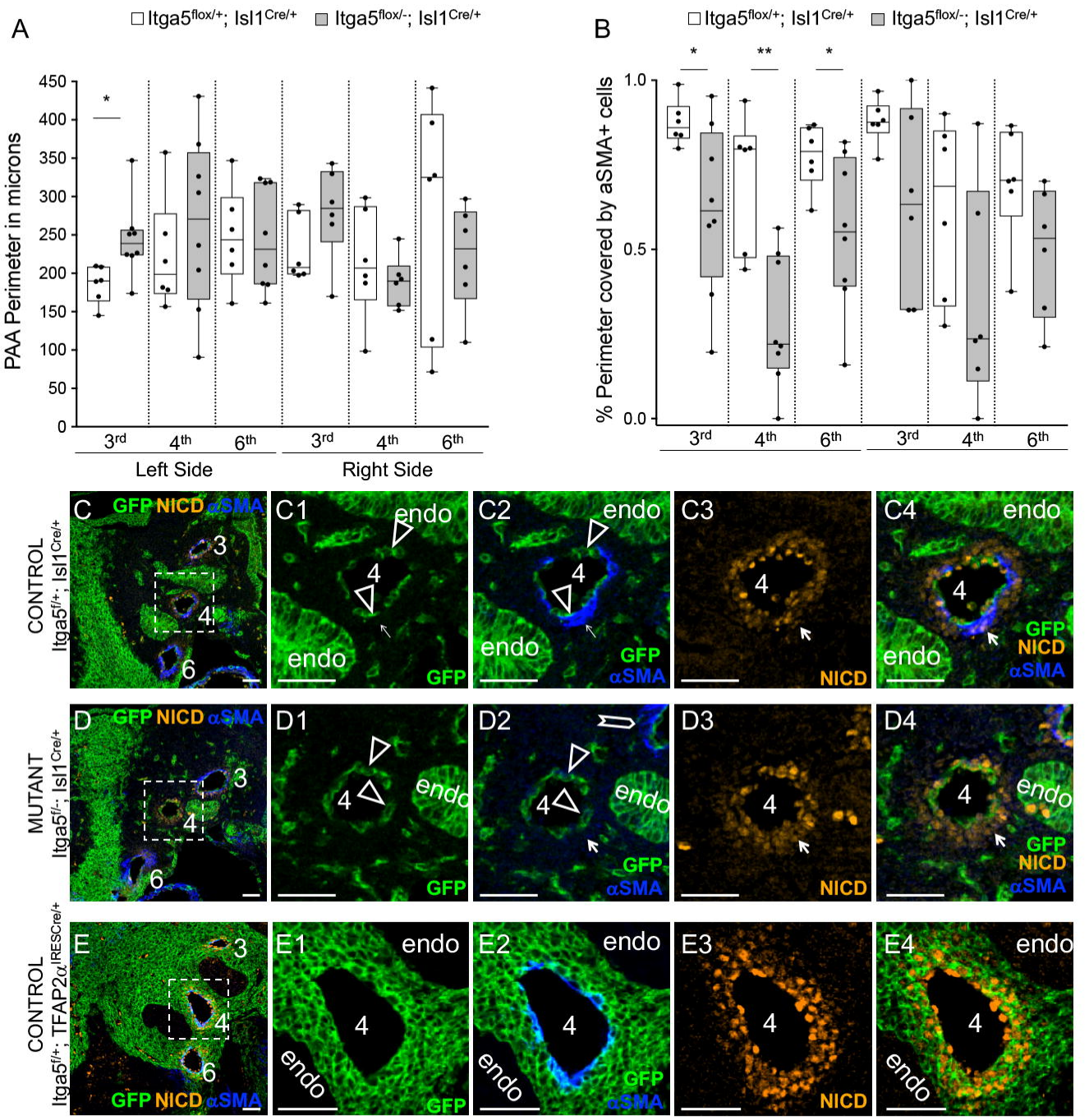

Figure 7. The expression of integrin α5β1 in the Isl1 lineages regulates the differentiation of neural crest-derived cells into VSCMs at E11.5 A. PAA perimeter has recovered in size in the mutants by E11.5. **B.** Smooth muscle coverage of the left 4th and left 6th PAA was deficient in the mutants. **C – D**. Despite defective differentiation of NC cells into VSMCs, the activation of Notch in the pharyngeal arch mesenchyme was not altered in the mutants. PAAs are numbered. PAA ECs at E11.5 are derived from the Isl1^{Cre} lineage (green, arrowheads in **C1, C2** and **D1, D2**). **C2 – D2**. VSMC differentiation assayed by the expression of alpha smooth muscle actin (αSMA, blue) is specifically affected around the 4th PAAs in the mutants (compare regions marked by the arrows in **C2** and **D2**). The activation of Notch assayed by the expression of NICD is not altered in the mutants with defective VSCM differentiation (arrows in **C3,C4** and **D3,D4**). **E.** Fate map using TFAP2α^{IRESCre} shows the location of NC-derived cells in the pharyngeal arches. Note extensive colonization of the mesenchyme between the endodermal pouches (endo) by the TFAP2α^{IRESCre} lineage. αSMA^{+} cells are GFP-negative in Isl1Cre strain (arrows in **C1-C2**). **E2**. αSMA^{+} cells are GFP+ in TFAP2α^{IRESCre} strain. All scale bars are 50 μm. Additional zoom-out views are in Sup. Fig. 6.

FIGURE 8

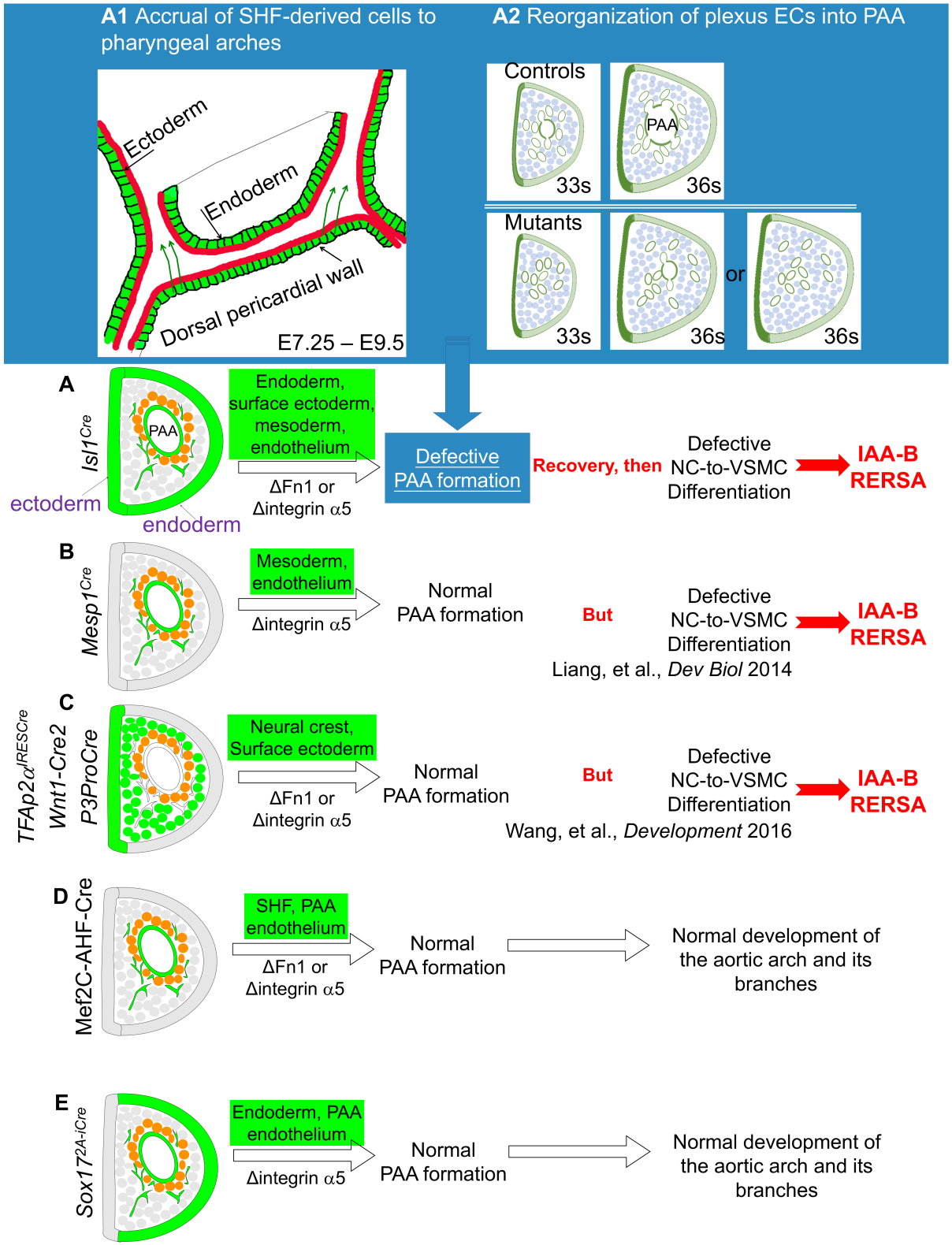

Figure 8. Cell – ECM interactions play essential roles at multiple stages during the development of the aortic arch and its branches. A – E. Depictions of coronal sections through the 4th pharyngeal arch at E10.5. Lineages are marked in green, NC-derived cells are depicted as circles, NC-derived cells next to the PAA endothelium are marked in orange. **A.** The expression of integrin α5β1 and Fn1 in the Isl1 lineages is required for the formation of the 4th PAAs (see **A1** and **A2** in the blue inset) as well as for NC-to-VSMC differentiation. The deletion of integrin α5 or Fn1 in the Isl1 lineages leads to IAA-B and RERSA. **A1 – A2.** Stages during which integrin a5 and Fn1 regulate the 4th PAA formation. **A1.** A schematic of Isl1 lineages (green) in the pharynx at E8.5 – E9.5. Green arrows indicate migration of splanchnic mesoderm cells into the pharyngeal arches. Red lines signify enriched localization of Fn1 protein at germ layer borders. Integrin α5β1 is expressed in all cell types in the pharynx at E8.5 (Chen et al., 2015) and regulates the accrual of pharyngeal mesoderm from the SHF (green arrows). **A2.** During the 10th day of mouse development, integrin α5β1 and Fn1 regulate the remodeling of the plexus endothelium in the 4th pharyngeal arch into the PAA. Isl1 lineages are marked in green. NC-derived cells are in blue. **B.** The expression of integrin α5 in the mesoderm regulates the differentiation of NC-derived cells into VSMCs. The deletion of integrin α5 in Mesp1 lineage, which includes the SHF, leads to defective NC-to-VSMC differentiation and results in the regression of the 4th PAAs leading to IAA-B and RERSA (Liang, et al., *Dev Biol* 2014). **C.** Fn1 becomes upregulated in NC-derived cells adjacent to the 4th PAA ECs between E10.5 and E11.5 The expression of integrin α5β1 and Fn1 in the NC-derived cells is required for NC-to-VSMC differentiation and the stability of the 4th PAA (Wang et al, 2016). The deletion of either integrin α5 or Fn1 in the NC (and the surface ectoderm) leads to IAA-B and RERSA but does not impair PAA formation. **D.** The expression integrin α5 or Fn1 in the SHF is not required for the morphogenesis of the aortic arch and its branches. **E.** The expression of integrin α5 in the endoderm and the pharyngeal endothelia is not required for the development of the aortic arch and its branches.

Supplemental Table 1. Itga5$^{f/f}$ x Itga5$^{+/-}$; Mef2C-AHF-Cre

Genotype	# Observed at Weaning
Itga5$^{f/-}$; Mef2C-AHF-Cre+	14 (22%)
Itga5 $^{f/-}$	12 (19%)
Itga5$^{f/+}$; Mef2C-AHF-Cre+	18 (29%)
Itga5 $^{f/+}$	19 (30%)
Total	63

Supplemental Table 2. Fn1$^{f/f}$ x Fn1$^{+/}$-; Mef2C-AHF-Cre

Genotype	# Observed at Weaning
Fn1$^{f/-}$; Mef2C-AHF-Cre+	23 (31%)
Fn1 $^{f/-}$	15 (20%)
Fn1$^{f/+}$; Mef2C-AHF-Cre+	17 (23%)
Fn1 $^{f/+}$	19 (26%)
Total	74